Summer 7-11-2019

EVALUATING FUTURE RESERVOIR STORAGE IN THE RIO GRANDE USING NORMALIZED CLIMATE PROJECTIONS AND A WATER BALANCE MODEL

Nolan T. Townsend
Earth and Planetary Sciences

Nolan Townsend

Candidate

Earth and Planetary Sciences

Department

This thesis is approved, and it is acceptable in quality and form for publication:

Approved by the Thesis Committee:

Dr. David S. Gutzler , Chairperson

Dr. Alex Mayer

Dr. Joseph Galewsky

EVALUATING FUTURE RESERVOIR STORAGE IN THE RIO GRANDE USING NORMALIZED CLIMATE PROJECTIONS AND A WATER BALANCE MODEL

by:

NOLAN T. TOWNSEND

B.S. GEOLOGY
UNIVERSITY OF TEXAS, 2013

THESIS

Submitted in Partial Fulfillment of the
Requirements for the Degree of

Master of Science
Earth and Planetary Sciences

The University of New Mexico
Albuquerque, New Mexico

July, 2019

Acknowledgments

This material is based upon work supported by the National Institute of Food and Agriculture, U.S. Department of Agriculture, under award number 2015-68007-23130, which made this research possible. I thank the U.S. Bureau of Reclamation for making their "Downscaled CMIP3 and CMIP5 Climate and Hydrology Projections" (archive at https://gdo-dcp.ucllnl.org/downscaled_cmip_projections/) available to me.

I acknowledge my adviser, Dr. David Gutzler, for all of the constructive criticism and positive feedback, expansive knowledge in earth sciences (and beyond), and the continued moral support throughout my Master's research. I would like to thank my committee members Dr. Joe Galewsky, and Dr. Alex Mayer for helping advance my understanding of the climate system and hydrology. A special thanks to Dr. Alex Mayer for allowing me access to his bucket model and his guidance on how to properly use and analyze his model. In addition, I want to express my gratitude to Dr. Phil King and Mr. Todd Blythe for their critical comments.

I acknowledge the World Climate Research Programme's Working Group on Coupled Modelling, which is responsible for CMIP, and I thank the climate modeling groups (listed in Table 1.1 of this paper) for producing and making available their model output. For CMIP the U.S. Department of Energy's Program for Climate Model Diagnosis and Intercomparison provides coordinating support and led development of software infrastructure in partnership with the Global Organization for Earth System Science Portals.

EVALUATING FUTURE RESERVOIR STORAGE IN THE RIO GRANDE USING NORMALIZED CLIMATE PROJECTIONS AND A WATER BALANCE MODEL

by

Nolan T. Townsend

B.S., General Geology, University of Texas, 2013

M.S., Earth and Planetary Sciences, University of New Mexico, 2019

Abstract

We develop and implement new tools for assessing the future of surface water supplies in downstream reaches of the Rio Grande, for which Elephant Butte Reservoir is the major storage reservoir. First, a normalization procedure is developed to adjust natural Rio Grande streamflows simulated by dynamical models in downstream reaches. The normalization accounts for upstream anthropogenic impairments to flow that are not considered in the model, thereby yielding downstream flows closer to observed values and more appropriate for use in assessments of future flows in downstream reaches. The normalization is applied to assess the potential effects of climate change on future water availability in the Rio Grande Basin at a gage just above Elephant Butte reservoir. Model simulated streamflow values were normalized force simulated flows to have the same mean and variance as observed flows over a historical baseline period, yielding normalization ratios that can be applied to future flows when water management decisions are unknown. At the gage considered in this study, the effect of the

normalization is to reduce all simulated flow values by nearly 72% on average, indicative of the large fraction of natural flow diverted from the river upstream from the gage.

The normalized streamflow scenarios are then implemented as the main boundary condition in a simple water balance model to analyze future policy options, using reservoir storage and downstream releases to compare management choices. It takes four years of twice the average annual inflow to fill Elephant Butte Reservoir to full operating capacity, starting from near-empty initial conditions as occurred in late 2018. In terms of increasing downstream releases and increasing reservoir storage, reducing direct reservoir evaporation was the best option from a strictly hydrologic perspective. Increasing the future inflows by reducing upstream diversions increases reservoir storage and Caballo releases, but there was also an increase in reservoir evaporation. Lastly, maintaining a minimum storage threshold for reservoir storage increases future average storage, but also leads to an increase in reservoir evaporation and a decrease in releases. Water stored in Elephant Butte Reservoir is lost via the positive correlation between increasing reservoir storage, and thus the increased surface area, and the subsequent rise in direct reservoir evaporation. Therefore, the water balance model suggests the most hydrologically efficient policy option involves reducing reservoir evaporation, although the water balance model does not consider the costs of methods to reduce evaporation.

TABLE OF CONTENTS

List of Tables

List of Figures

Chapter 1: Normalizing Simulated Streamflow

I. Introduction

Climate change impacts flows in major rivers very substantially **(**Gosling et al. 2010; Reclamation 2016). Dynamical model simulations of future climate change play an increasingly important role in the development of water policy to adapt to ongoing climate change (Arnell et al. 2011, Howells et al. 2013). However, streamflow is not a standard output variable in the global models used for national and international climate change assessment. Streamflow projections derived from dynamical climate models must couple the climate model output to a surface water model that uses climate model output variables as input. The resulting simulated streamflow values describe hydrologic systems that represent naturally occurring flows.

These simulations should yield streamflows directly comparable to gaged flows in headwaters basins, where anthropogenic impairments to flows are minimal. In downstream reaches, however, model-simulated flows cannot be compared directly with observations, because climate models do not incorporate anthropogenic diversion and management of water. Many rivers are used extensively for agriculture and drinking water, with heavily managed flows blocked by dams such that downstream flows are entirely controlled. Management of streamflow is often guided by agreements that govern downstream flow requirements.

This paper describes a straightforward statistical approach to account for anthropogenic management in model-simulated streamflows, appropriate for flows that

are known to have been impacted by upstream dams and diversions. The parameterization of human impacts to flows, developed using historical observations, can be applied to simulations of future flows in which human water management decisions are not known. The procedure allows model projections of future (natural) flows to be "normalized", so that downstream flow projections more closely represent the flows relevant to water policy decisions in downstream reaches.

The procedure we develop here is conceptually the inverse of "naturalizing" gaged flows, a common practice for the purposes of water supply outlook forecasting (NRCS, 2011) or for adaptation of gaged flows for the development of paleoclimatic streamflow reconstruction based on proxy data (e.g. Woodhouse et al. 2016). Unlike operational naturalization, which explicitly tracks anthropogenic inputs and outputs along the length of a river (NRCS, 2011), we choose to account for human flow impairments using a simple statistical strategy that accounts for all upstream impairments using two empirically derived constants. These constants are the values needed to force the multi-year mean and interannual variance of simulated flows to match the mean and variance of gaged flows over a historical baseline period.

There are two reasons for using a parameterization approach rather than following a more precise and explicit accounting of impairments. First, we seek to develop a normalization strategy that can be adapted quickly and relatively easily to any river system, without documentation of all the impairments -- a difficult task requiring detailed knowledge of management practices along the river in question. Second, the principal goal of the parameterization is to apply it to projected future flows, for which the management decisions that need to be accounted for are unknown.

The normalization developed here is applied to flows at San Marcial, a gaged location on the middle Rio Grande in New Mexico, USA. This site is located just upriver from Elephant Butte Reservoir, the major storage reservoir on this stretch of the river (Fig. 1). Flows at the San Marcial gage are far from the headwaters of the Rio Grande, and the effects of management on the observed flow at San Marcial cannot be ignored (Mix et al, 2012; Blythe and Schmidt, 2018).

We apply the normalization procedure to streamflow simulations developed by the U.S. Bureau of Reclamation (BoR) as part of its West Wide Climate Risk Assessment project (Reclamation 2013). BoR has utilized coarse-resolution projected climate data and statistically bias corrected and downscaled these data to make the model output useful for hydrologic modeling at a regional scale (Pielke et al. 2012; Reclamation 2013). Vertical fluxes of water produced by the downscaled climate simulations are fed into the Variable Infiltration Capacity surface hydrology model (Liang et al. 1994; Gao et al. 2010), where water is routed between grid cells and into and out of the surface.

Section II of this paper presents a short summary of the BoR streamflow simulations. Section III documents the impact of trans-mountain diversions on the native observed flow values. Sections IV outlines the normalization procedure applied to model output. Section V shows the results of the normalization procedure and the how the normalized flow values compare to observed flows and simulated natural streamflow values. Discussion and conclusions follow in sections VI and VII.

II. Observed and Simulated Streamflow Data

We use simulated flows generated by BoR for the "Elephant Butte Dam" pour point (EBD; Fig. 1) on the Rio Grande, and develop a normalization procedure to adapt the simulated flows to actual flows at San Marcial, a short distance upriver. Instead of explicitly accounting for consumption and diversions using a management model capable of simulating future water management decisions, we parameterize anthropogenic effects using statistical normalization constants that force the annual mean and interannual variance of simulated flows at EBD to match the mean and variance of observed flows in recent decades at San Marcial. This procedure is described in Sections III and IV.

Flow at San Marcial has been split into two channels, so there are two streamgages present at this point in the river: one denoted the Rio Grande Floodway (USGS 08358400) and the other denoted the Rio Grande Conveyance Channel (USGS 08358300). The conveyance channel was constructed upstream of Elephant Butte Reservoir to help New Mexico meet its interstate delivery obligations by increasing the hydraulic efficiency of the channel. The total flow value at San Marcial is the sum of flows at these two gages.

Global climate model output is taken from the Fifth Coupled Model Intercomparison Project (CMIP5) by the World Climate Research Programme. These models produce long term simulations of global climate out to the end of the 21st century. Following CMIP5 protocols, the simulations are driven by historical climate forcings from 1951-2005, and thereafter by one of several prescribed emission scenarios that represent future greenhouse gas concentrations based on an array of possible socio-economic story lines (Taylor et al. 2012; IPCC, 2013). Importantly, the prescribed

anthropogenic emissions provide the main forcing in the climate models that evolve over space and time. The CMIP5 simulations considered here are driven by the following four emissions scenarios: RCP 2.6, RCP 4.5, RCP 6.0, and RCP 8.5, ordered from low to high perturbation to Earth's surface energy budget (Taylor et al. 2012; IPCC, 2013).

CMIP5 climate model output is typically archived at coarse resolutions of 1 to 2 degrees. Raw model output, including temperature and precipitation, needs to be downscaled and bias corrected to be useful at a local scale and provide data at finer resolution. The BoR has bias corrected and statistically downscaled (BCSD) data available at a 1/8-degree resolution at a monthly timestep, which are used in this study (Reclamation, 2013, 2014).

Streamflow simulations based on the BoR BCSD climate output are achieved using a routing model (VIC; Liang et al. 1994) that moves water from one grid cell to another and into/out of the surface, which ultimately produces monthly simulated streamflow (Gao et al. 2010; Reclamation, 2014). Importantly, the flow produced by the VIC model simulates streamflow without the influence of human impairments on streamflow. For this reason, the flows produced from the VIC model are interpreted as naturalized flows at the Elephant Butte Dam pour point.

The BoR archive of CMIP5-forced streamflow projections includes 97 simulations based on 31 different climate models. In this paper we will present a selection of results based on sixteen of the simulations: one each from four different models forced by four different RCP scenarios (Table 2).

III. Trans-Mountain Diversions

Actual flow in the middle Rio Grande is augmented by input of water from trans-mountains diversions, or imported water. We consider trans-mountain diversions separately from the management of native water in the river basin, because these diversions are typically accounted for separately from native water in operational water management accounting. In the upper Rio Grande basin, the principal transfer occurs from the San Juan River (a tributary of the Colorado River) upstream from San Marcial. The Azotea Tunnel gaging station indicates the main import location (Fig. 1). The Rio Grande Compact Commission publishes a report each year, documenting the imported water by month and with an annual total (http://www.ose.state.nm.us/Compacts/RioGrande/isc_rio_grande_tech_compact_reports.php).

We used the cumulative annual imported water data from these reports for the period 1971-2015 and subtracted annual imported water from the observed flows at San Marcial for each year over the same period to represent native flow at San Marcial (Fig. 2). We did not attempt to parameterize the management of imported water upstream from San Marcial. The relationship between annual native and imported flows in this data record is nonlinear: when native flows are low, more water is imported. We opted for a simple empirical threshold that distinguishes annual imported water during drier and wetter years. Figure 2 shows that when native flows fall below the 13.45 m^3/s threshold (black dashed vertical line), the annual average flow of imported water is 4.78 m^3/s (horizontal solid orange line and blue dots). Native flows greater than the 13.45 m^3/s

threshold are associated with a lower annual mean imported flow of 1.79 m^3/s (horizontal solid red line and black dots).

Prior to the normalization, we remove the imported flows from the observed flows, so that the observed data are comparable to the simulated San Marcial streamflow data which do not include imported water. This was accomplished by first determining if the observed (minus imported) flow was above or below the 13.45 m^3/s threshold. Then, we use the average value of imported water above (1.79 m^3/s) or below (4.78 m^3/s) the 13.45 m^3/s threshold and subtract that imported water value from the observed flow value for each year (Fig. 2). Then, we implement the normalization procedure described in Section IV, and finally add back an annual value of imported water based on the newly normalized flow based on its relation to the threshold value of 13.45 m^3/s.

The treatment of trans-mountain diversions can be summarized as follows.

Let $Q_o(j) =$ observed annual flow at San Marcial for year j, and $Q_{SJ}(j) =$ annual imported water data from the Rio Grande Compact Commission Reports: We remove imported water to get annual native flow at San Marcial $Q_{RGO}(j)$:

$$Q_{RGO}(j) = Q_o(j) - Q_{SJ}(j)$$

Overall, we find that including imported water in our calculation modestly decreases normalized high flow values, but it also provides a slight buffer during the lower flow years (Fig. 2). Our normalization procedure maintains the two average values of imported water shown in Figure 2 into the future, thereby assuming that imported water is supplied to the Rio Grande at historical rates in the future, impacting future San Marcial streamflow as in the past.

IV. Normalization Procedure for Naturalized Flows

Observed data from the pair of gages at San Marcial are considered to represent total inflows into storage at Elephant Butte Reservoir. Likewise, the simulated flows at the Elephant Butte Dam pour point are interpreted after normalization as San Marcial flows, as mentioned in Section II. The normalization is based on adjusting the average and interannual variability of annual simulated flows to match the average and variability of observed native flows over a 50-year baseline period (1964-2013). The constants needed to accomplish this adjustment are then applied to future simulated annual values.

As a first step, we convert the observed distribution of annual native flows $Q_{RGO}(j)$ to a log-normal distribution $Q'_{RGO}(\mathrm{j}) = \ln\left(Q_{RGO}(j)\right)$ that has mean $\overline{Q'_{RGO}}$ and variance $\sigma^2\left(Q'_{RGO}\right)$. The log normalization accounts for positive skewness in the distribution of flows (Brutsaert, 2005). Similarly, we log-normalize the time series of a simulated annual flow at "Elephant Butte Dam" $Q_s(j)$ and calculate the mean and variance of log-normalized simulated values $Q'_s(\mathrm{j})$:

$Q'_s(\mathrm{j}) = \ln\left(Q_s(j)\right)$; with mean $\overline{Q'_s}$ and interannual variance $\sigma^2\left(Q'_s\right)$

The first normalization constant *a1* is the difference in means between observed and simulated log-normalized flow distributions

$$a1 = \overline{Q'_{RGO}} - \overline{Q'_s} \qquad [1]$$

Applying *a1* to log-normal simulated flows yields a bias-adjusted time series of simulated flows $Q'_D(j)$:

$$Q'_D(j) = a1 * Q'_s(j); \qquad [2]$$

The bias-adjusted flows have a mean value $\overline{Q'_D}$ that, by construction, is equal to $\overline{Q'_{RGO}}$. The "bias" here mostly represents water diverted for consumptive use upstream of San Marcial.

In addition, we normalize the variance of the bias-corrected, simulated log-normalized flows during the historical period. This step is taken because, in addition to exhibiting much greater average flow, the distributions of simulated annual flows are observed to exhibit much greater interannual variability than the observations.

The ratio of the standard deviations of observed to simulated flows, over the 50-year baseline period, yields a variance normalization constant:

$$a2 = \left(\frac{\sigma(Q'_{RGO})}{\sigma(Q'_s)}\right) \qquad [3]$$

Normalized annual simulated flows are then calculated using the constants a*1* and a*2* to force the log-normal distributions of the observed and simulated time series to have the same time mean and variance over the historical baseline period.

$$Q'_N(\mathrm{j}) = \left(Q'_s - \overline{Q'_D}\right) * a2 \; + \; \overline{Q'_D} \qquad [4]$$

Exponentiate to undo the log transform, returning flows with the correct physical units:

$$Q_N(j) = exp\left(Q'_N(\mathrm{j})\right);$$

The final step in the normalization process is to reintroduce an estimated value of imported water from trans-mountain diversions. Imported water is added to the normalized values based on the threshold flow value established in Section III (Fig. 2). The conditions are as follows:

$$\begin{cases} if\ Q_N(j) < Q_{Threshold}; & then\ Q_{SN}(j) = Q_N(j) + Q_{SJ\_Low} \\ if\ Q_N(j) > Q_{Threshold}; & then\ Q_{SN}(j) = Q_N(j) + Q_{SJ\_High} \end{cases}$$

where: $Q_{Threshold} = 13.45\ m^3/sec$

The time series of normalized flows $Q_{SN}(j)$ at San Marcial accounts for systematic model bias in reproducing streamflow, the depletion of natural native flows by dams and diversions upstream of San Marcial, and the modest bias associated with the difference in location between the observed flow measurement point at San Marcial and the simulated pour point downstream at Elephant Butte Dam (Fig. 1). The resulting normalized flows do not match the statistics of the observations in all respects. In particular, the distributions of both observed flows and normalized simulated flows exhibit positive third moments (skewness), but the normalized flow distributions for the different simulations tend to have higher skewness than the observations. Thus our estimates of extreme high annual flows at San Marcial in the model simulations may exhibit larger values, in both the historical and projected future periods, than historical observations suggest is likely.

Fixing the normalization constants ($\overline{Q'_D}$ & σ ratio; Equations 1 and 3) for future simulated flows implies that the effects of human management on the mean and interannual variability statistics of Rio Grande annual flows at San Marcial do not change with time. Changes to these constants could be prescribed, which would be interpreted as representing changes to water management upstream.

The normalization approach modifies model output so that the simulated flows are comparable to observed, diversion-impacted flows. As a result, the model output can be used for assessments of the impacts of future climate scenarios for the region downstream of San Marcial, an area of intensive irrigated agriculture dependent on

releases from Elephant Butte and Caballo Reservoirs (tan-shaded region in Fig. 1; Ward et al. 2019).

V. Results: Normalization of Annual Flows at San Macial

Figure 3 illustrates the difference between simulated, normalized and observed flow values from 1964-2013, the period over which the normalization was defined. The HAD85 simulation (Jones et al. 2011) is portrayed by the black dotted line (simulated) and the red solid line (normalized). The mean observed flow (blue solid line) is about 26% of mean simulated flow yielded by this particular simulation during the historical baseline period. The ratio of normalized and simulated flows is similar to the value found by Blythe and Schmidt (2018), who naturalized observed San Marcial flows by explicitly accounting for human impairments. Conceptually, their procedure is the inverse of our treatment of simulated flows, but like most naturalization algorithms it is based on explicit specification of flow impairments, rather than our parameterized approach.

Figure 4 is like Figure 3, except that annual average flows are plotted for the 1964-2070 period. All 97 model simulations are shown using light gray dots. The variability of the normalized flow values in the HAD85 simulation (red line) decreases over the last 30 years of the timeseries (2041-2070). This simulation does not generate a monotonic decline in flow as climate warms up as the result of RCP8.5 radiative forcing. For example, from 2011-2040 the cumulative sum of the normalized flow values in the HAD85 increase slightly relative to 1981-2010 period. However, the cumulative sum of normalized simulated flows (in the HAD85 simulation) decreases by about 38% by from 2041-2070 when compared with the total flow from 1981-2010 period. This reveals much lower flows in the study area as climate warms and the southwest transitions to a more arid climate. The decrease in streamflow in this assessment is more than double the decrease in streamflow found by Hurd and Coonrod (2012) where streamflow in the

middle Rio Grande is predicted (in a different model simulation) to decrease by approximately 22-27% by 2080. However not all simulations exhibit such declines in future flows, as depicted by the cloud of gray dots.

We compare the following three normalized flow scenarios in Figure 5: HAD85 simulation as already discussed (solid red line), MIR26 (black dot-dashed) line and ACC85 (dashed orange line). The gray dots in the background are annual normalized flows from all available model simulations as in Fig. 4. MIR26 represents the highest average flow among all normalized projections over the 1960-2100 period (about 47.2 m^3/s), HAD85 represents an intermediate level of flow decline (24.4 m^3/s), and the lowest flows on average, are found in ACC85 (21.6 m^3/s). The MIR26 simulation exhibits exceptionally high variability in flows towards the end of the century. The ACC85 and HAD85 simulations exhibit an overall decrease in normalized flows and decreased variability towards the end of the century.

The boxplots in Figure 6 show the interannual distributions of observed streamflow (light blue) and the normalized simulated flows for the HAD85 simulation (orange) and the MIR26 simulation (gray), for recent and future periods (1964-2013 and 2021-2070). The period 1964-2013 is the historical baseline we used to calculate the normalized values. Five additional simulations were selected at random for comparison over these same time periods and are plotted in Figure 6. By construction the mean and variability of the observed data matches the variability seen in the normalized flows, but the full range of variability is different even in the historical period.

In future decades some simulations maintain or increase variability compared to the baseline period, while other simulations exhibit dramatic decreases. The most notable

decrease in variability among all models is noted in the ACC85 model simulation during the 2045-2070 period. Conversely, MIR26 exhibits an increase in both variability and average streamflow during the same period. The difference in projected flows between models and different RCP scenarios is highlighted in Figure 7, where the change in average flows towards the end of the century is illustrated. Again, the HAD85 and ACC85 (not shown) are "drier" models across all RCP scenarios while MIR26 is "wetter" across all RCP scenarios. Figure 7 represents a subset of 16 models that include all four RCP scenarios where we calculated a 50-year mean difference between projected streamflow later this century (2021-2070) and earlier this century (1971-2020). Within this subset of model, we found that 62% of the variance of streamflow trends among all simulations is accounted for by model-to-model differences, not RCP differences or natural variability.

Taken together, averaged over all 16 models for which we have 4 RCP-driven scenarios, the normalized streamflow is projected to decrease slightly (Fig. 8). The higher the RCP scenario, the lower the flows are on average, and the lower the interannual variability is, in the later years of the 21st Century. This is illustrated by comparing the solid blue line (RCP 2.6) and the solid red line (RCP 8.5). Thus, large model to model variability is present due to factors such as different representations of physical processes (e.g. clouds and precipitation) in each model, and sampling uncertainties associated with natural variability.

VI. Discussion

The modelled flow output generated by the BoR simulations (Reclamation 2014) represents a naturalized streamflow so the simulated values must be bias corrected to provide realistic flows in downstream reaches out into the future. The normalization procedure described here accounts for management of the Rio Grande upstream of the San Marcial gaging sites through a statistical parameterization of the simulated BoR flows by relating the mean and standard deviation of the observed timeseries to the simulated timeseries, as outlined in Section IV. On average, the simulated BoR flows are reduced by 72% across all model simulations and RCP scenarios.

Each model projection includes internal natural variability that is often ascribed to the uncertainty in and among climate models. This is one of the reasons there is much model to model variability in figures 5,6, and 7. Each climate model projection shown in this paper is only one realization borne out of a range of natural variability that could potentially occur (Deser et al. 2012). Figure 8 illustrates that streamflow changes associated with four RCP scenarios, each with a 16-member ensemble, are difficult to distinguish until the trends emerge from the noise, or natural variability, after about 2070. Additionally, some of the model to model variability originates from different equations used to simulate features such as clouds within each modelling groups' global climate model (IPCC, 2013).

The models are not constrained to match observations each year, because the CMIP5 models are freely running and generate their own natural variability: ENSO cycles, pluvial and drought years, etc. The 50-year length of the baseline period (1964-2013) is designed to be sufficient to capture the statistics of natural variability on

interannual and decadal time scales. Nevertheless, it is important not to interpret these simulated flow time series as forecasts for individual years or decades.

One important limitation of the normalization procedure is the presence of positive skewness that the normalization procedure does not directly address. This means that it may be difficult to realistically interpret the wet-year outliers. Additionally, the normalization constants used here do not evolve with time and therefore will not reflect evolving water management practices, or any other anthropogenic changes other than greenhouse gas emissions, that occur upstream in the future. Adjusting the normalization constants could be implemented to parameterized significant management changes, such as to the Rio Grande Compact or the Rio Grande Operating Agreement of 2008 (Reclamation 1939; Reynolds et al. 1974; Reclamation 2008), that would affect flows at San Marcial.

VII. Conclusion and Final Remarks

We have created a simple statistical method for adapting model-simulated future streamflows to generate downstream flow projections with realistic magnitudes in a major river that is heavily managed. The goal of the normalization is to account for the cumulative impact of humans on upstream flows using a simple statistical normalization method. We apply the normalization to translate simulated flows in the middle Rio Grande into flow values appropriate for use as inflows into the major storage reservoir on the river.

The effect of the normalization procedure applied to San Marcial annual flows is to reduce simulated flows by nearly 72% on average during the historical baseline period, confirming that human engineering projects, diversions, and reservoirs drastically reduce the natural flows one might expect in the absence of human management (Blythe and Schmidt 2018).

Model to model variations still exist and are attributed to climate model parameterization schemes, differences in spatial resolution, random atmospheric variability, etc. in the original climate model simulations. Based on the subset of 16 models each containing 4 RCP scenarios (Fig. 7), 62% of the variance of streamflow trends among all simulations is accounted for by model-to-model differences, not RCP differences or natural variability. Therefore, a method to constrain model to model variance is needed to explore which models are best suited this study area.

Consequently, the normalization procedure yields model-generated future streamflow scenarios that can be used by policy makers and stakeholders on a regional scale downstream of Elephant Butte Reservoir. The normalized streamflows are suitable

for use as inputs to assessments that consider for future water management options in this region. The normalized flows described in this study are generated at an annual timestep, but the same technique could be adapted to monthly simulated flow values as well.

Tables

Table 1.1 List of CMIP5 climate models used.

Modeling Center (or Group)	Institute ID	Model Name
Commonwealth Scientific and Industrial Research Organization (CSIRO) and Bureau of Meteorology (BOM), Australia	CSIRO-BOM	ACCESS1.0 ACCESS1.3
Beijing Climate Center, China Meteorological Administration	BCC	BCC-CSM1.1
Canadian Centre for Climate Modelling and Analysis	CCCMA	CanESM2 CanCM4 CanAM4
National Center for Atmospheric Research	NCAR	CCSM4
Community Earth System Model Contributors	NSF-DOE-NCAR	CESM1(BGC) CESM1(CAM5)
Centre National de Recherches Météorologiques / Centre Européen de Recherche et Formation Avancée en Calcul Scientifique Commonwealth Scientific and Industrial Research Organization in collaboration with Queensland Climate Change Centre of Excellence EC-EARTH consortium	CNRM-CERFACS CSIRO-QCCCE EC-EARTH	CSIRO-Mk3.6.0
Centre National de Recherches Météorologiques / Centre Européen de Recherche et Formation	CNRM-CERFACS	FGOALS-g2 FGOALS-gl

Avancée en Calcul Scientifique Commonwealth Scientific and Industrial Research Organization in collaboration with Queensland Climate Change Centre of Excellence EC-EARTH consortium LASG, Institute of Atmospheric Physics, Chinese Academy of Sciences and CESS,Tsinghua University LASG, Institute of Atmospheric Physics, Chinese Academy of Sciences	CSIRO-QCCCE EC-EARTH LASG-CESS LASG-IAP	FGOALS-s2
The First Institute of Oceanography, SOA, China	FIO	FIO-ESM
NOAA Geophysical Fluid Dynamics Laboratory	NOAA GFDL	GFDL-CM3 GFDL-ESM2G GFDL-ESM2M
NASA Goddard Institute for Space Studies	NASA GISS	GISS-E2-H-CC GISS-E2-R GISS-E2-R-CC
National Institute of Meteorological Research/Korea Meteorological Administration	NIMR/KMA	HadGEM2-AO
Met Office Hadley Centre (additional HadGEM2-ES realizations contributed by Instituto Nacional de Pesquisas Espaciais)	MOHC (additional realizations by INPE)	HadGEM2-CC HadGEM2-ES

Institute for Numerical Mathematics	INM	INM-CM4
Institut Pierre-Simon Laplace	IPSL	IPSL-CM5A-MR IPSL-CM5B-LR
Japan Agency for Marine-Earth Science and Technology, Atmosphere and Ocean Research Institute (The University of Tokyo), and National Institute for Environmental Studies	MIROC	MIROC-ESM MIROC-ESM-CHEM
Atmosphere and Ocean Research Institute (The University of Tokyo), National Institute for Environmental Studies, and Japan Agency for Marine-Earth Science and Technology	MIROC	MIROC5
Max-Planck-Institut für Meteorologie (Max Planck Institute for Meteorology)	MPI-M	MPI-ESM-MR MPI-ESM-LR
Meteorological Research Institute	MRI	MRI-CGCM3
Nonhydrostatic Icosahedral Atmospheric Model Group	NICAM	NICAM.09
Norwegian Climate Centre	NCC	NorESM1-M

Table 1.1. List of all climate models from their respective modeling groups that were analyzed.

Table 1.2 List of models shown in the Figures.

Full Name	Abbreviated
access1-0_r1i1p1	ACC26
bcc-csm1-1_r1i1p1	BCC26
ccsm4_r1i1p1	CCSM26
cesm1-cam5_r1i1p1	CESM26
csiro-mk3-6-0_r1i1p1	CSIRO26
fio-esm_r1i1p1	FIO26
gfdl-cm3_r1i1p1	GFC26
gfdl-esm2g_r1i1p1	GFEG26
gfdl-esm2m_r1i1p1	GFEM26
giss-e2-r_r1i1p1	GISS26
hadgem2-ao_r1i1p1	HAO26
hadgem2-es_r1i1p1	HAD26
ipsl-cm5a-mr_r1i1p1	IPSL26
miroc5_r1i1p1	MIR26
miroc-esm-chem_r1i1p1	MIRC26
miroc-esm_r1i1p1	MIRE26
noresm1-m_r1i1p1	NOR26

Table 1.2. Simulation naming convention for select model simulations. The number 26 after the abbreviated terms reflects the RCP scenario and the 26 is just used as a place holder. Values could be 26,45,60, or 85. Models referenced in Figure 5 are shaded light gray.

Figures

Figure 1.1 Overview of the study area.

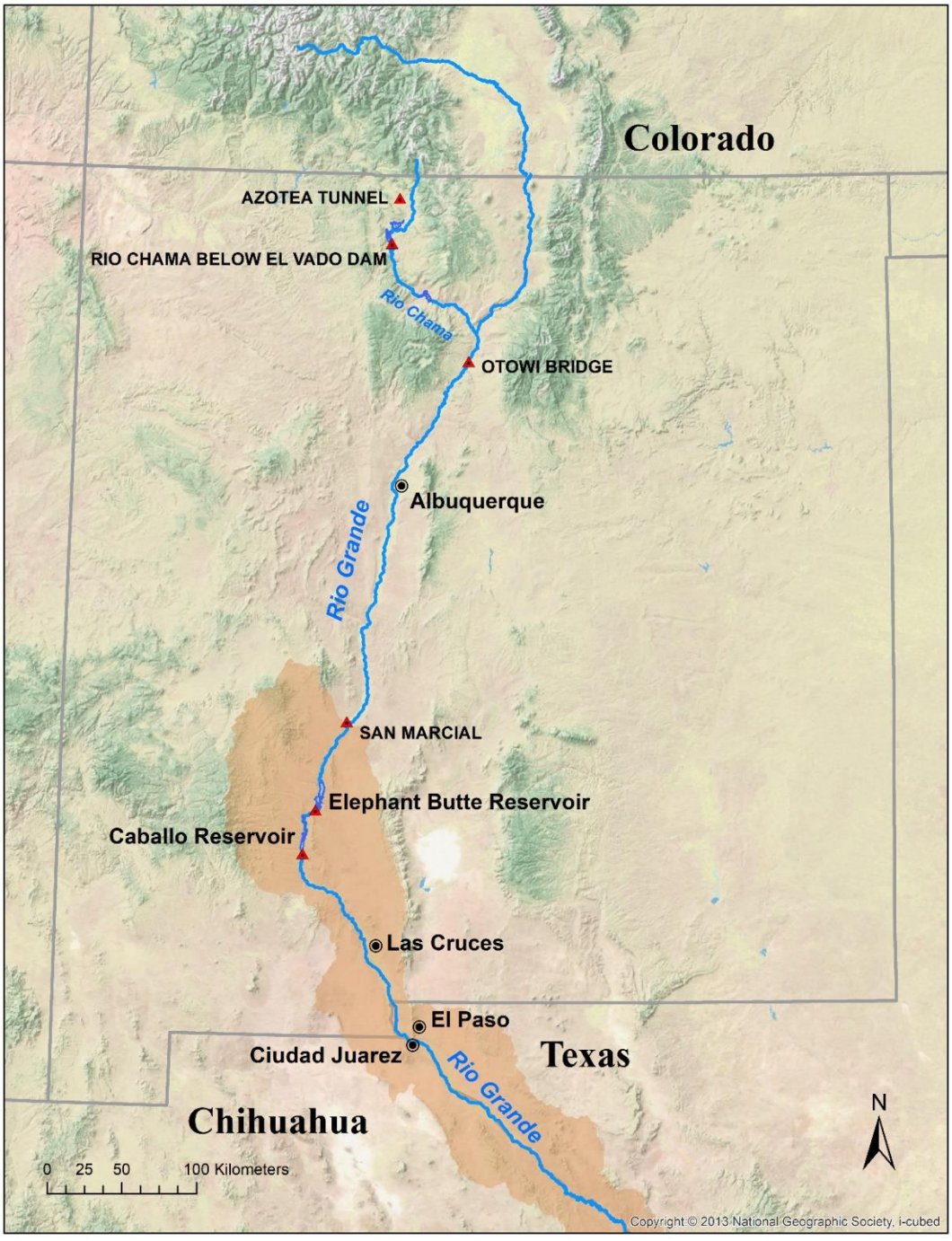

Figure 1.1. Overview map of the upper Rio Grande ranging from the headwaters region in southern Colorado downstream into Texas. Red triangles designate USGS streamgage locations. Black dots indicate city locations. The principal trans-mountain diversion into the Rio Grande basin occurs through Azotea Tunnel in northern New Mexico. Tan shading represents the valley of the Rio Grande downstream of San Marcial.

Figure 1.2 Annual trans-mountain diversions.

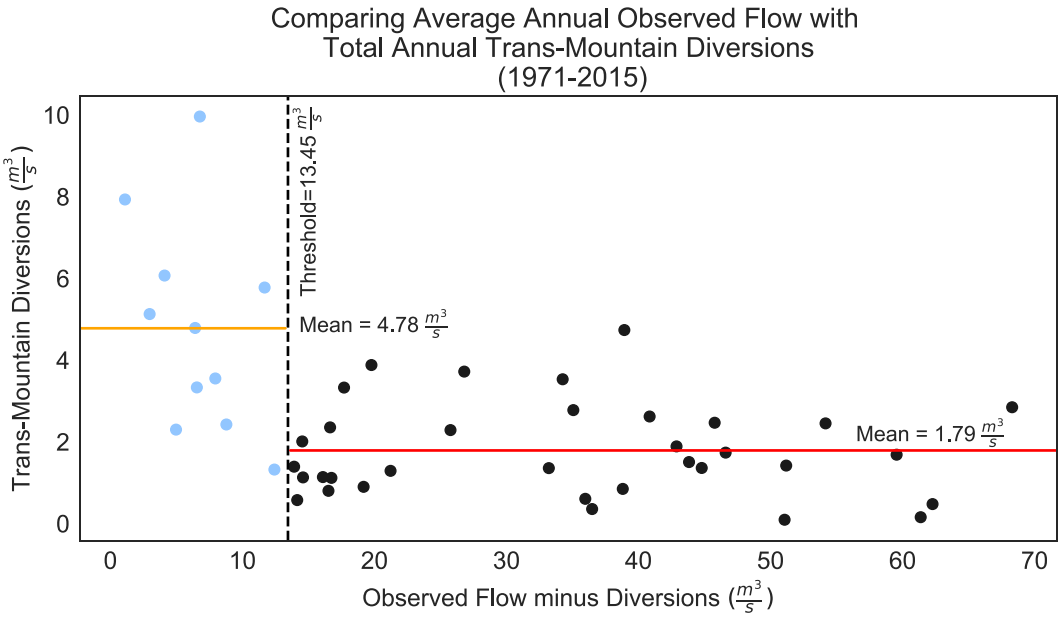

Figure 1.2. Annual average flows of trans-mountain diversions (y-axis) plotted against annual average observed flows at San Marcial with diversions subtracted. The x-axis therefore represents native flow at San Marcial. A break point is defined at a threshold value of 13.45 m^3/sec (vertical black dotted line) to distinguish low flow years (<13.45 m^3/s, blue dots) from normal to higher flow years (>13.45 m^3/s, black dots).

Figure 1.3 Annual timeseries comparison over historical baseline period.

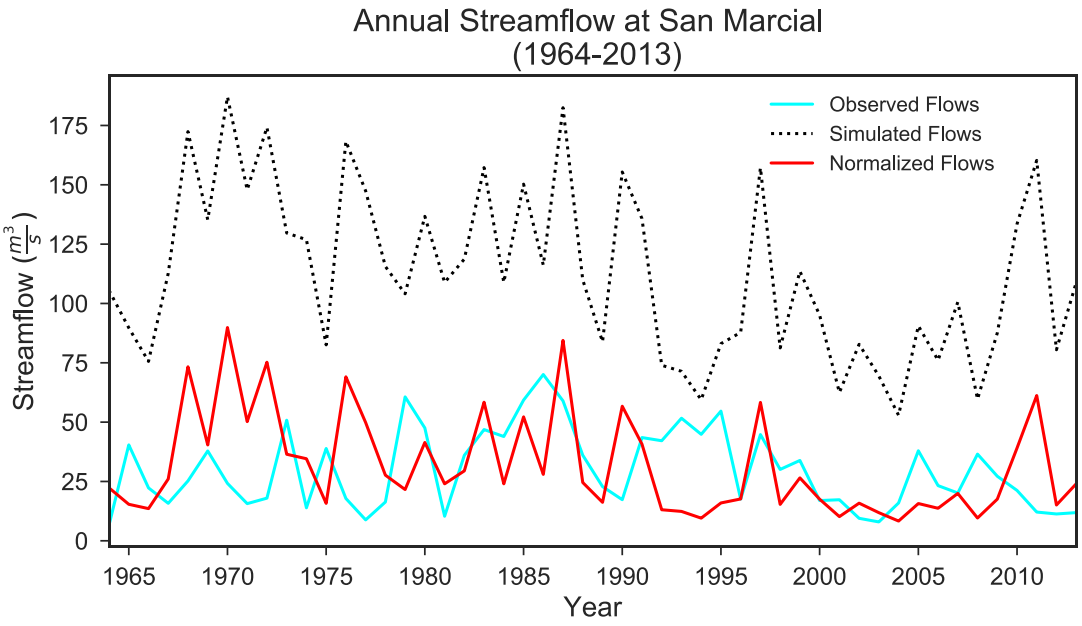

Figure 1.3. Annual time series of simulated flow (black dotted line), total observed flows at San Marcial (cyan), and normalized simulated flows (red) for the 50-year historical base line period (1964-2013). The lines for simulated and normalized flows are derived from the HAD85 simulation.

Figure 1.4 Annual timeseries comparison of all models from 1964-2070.

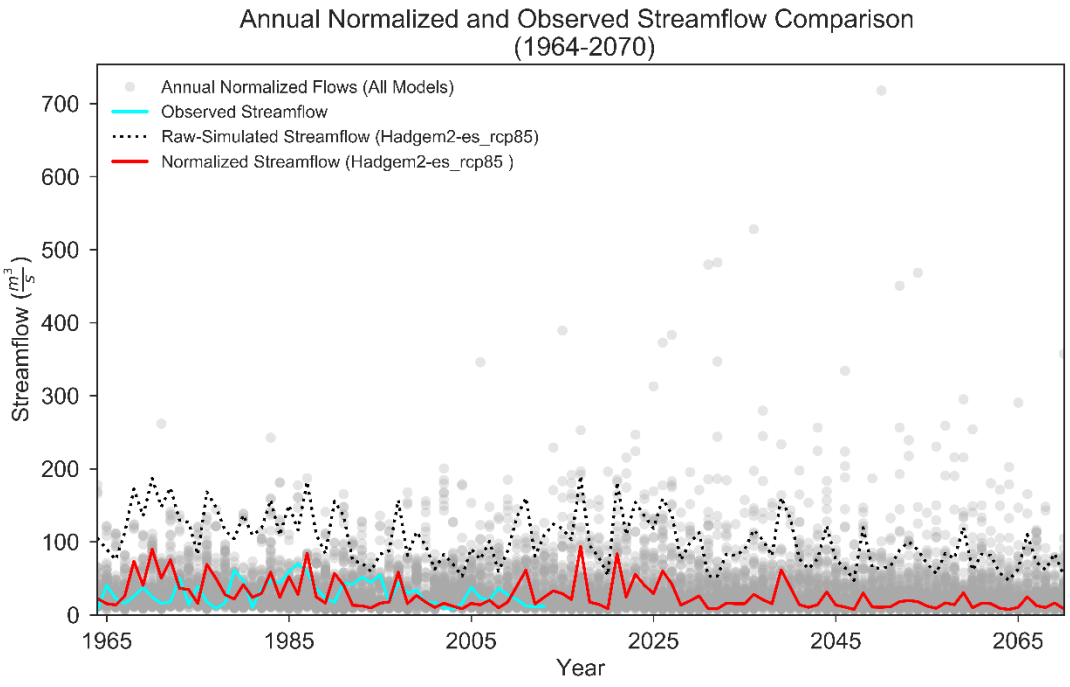

Figure 1.4. Annual flow values at San Marcial for observed flows (cyan, 1964-2013), simulated flow values (prior to normalization) for the HAD85 simulation (black dashed line), normalized flows for the HAD85 simulation (red line), and normalized annual flows for all 97 simulations (gray dots).

Figure 1.5 Annual normalized streamflow comparison (1960-2100).

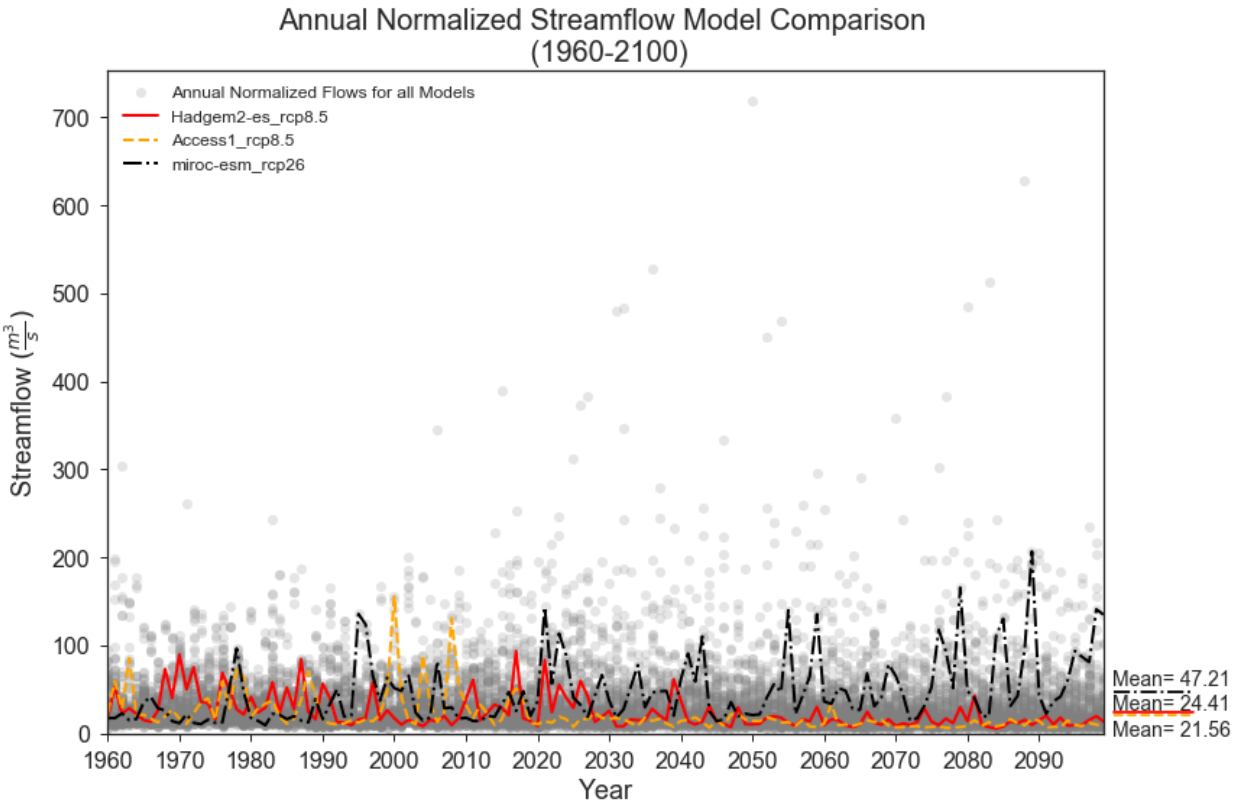

Figure 1.5. Normalized annual flows (gray dots) for all simulations considered. The HAD85 values are shown as a solid red line, the MIR26 values are shown by the black dot-dashed line, and the ACC85 simulation is shown as an orange dashed line. The mean values averaged over the entire 141-year period for these three models are shown to the right of the figure.

Figure 1.6 Normalized flow distributions for two 50-year time periods.

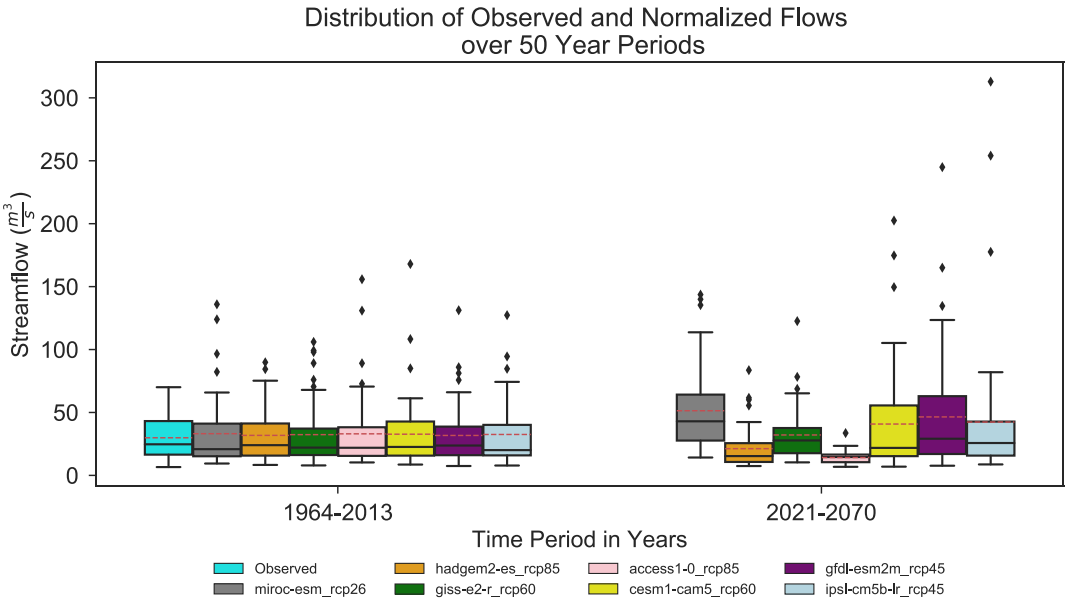

Figure 1.6. Boxplots showing the distribution of annual normalized flows for two separate 50-year periods: (left) the historical period 1964-2013, and (right) projected flows for 2021-2070. The median value is shown by a solid black line in the center of each box and. The whiskers represent anomalous values that are 1.5*IQR from the 25th and 75th percentile, respectively. Outliers are represented as black diamonds. Mean values over each period are shown as red dashed lines within each box. The distribution of observed annual flows (in cyan) is shown first among the historical distributions. The orange fill represents the HAD85 simulation and the gray represents the MIR26 simulation, discussed in Section IV. Five additional simulations are shown for comparison.

Figure 1.7 Normalized streamflow 50-year period differences.

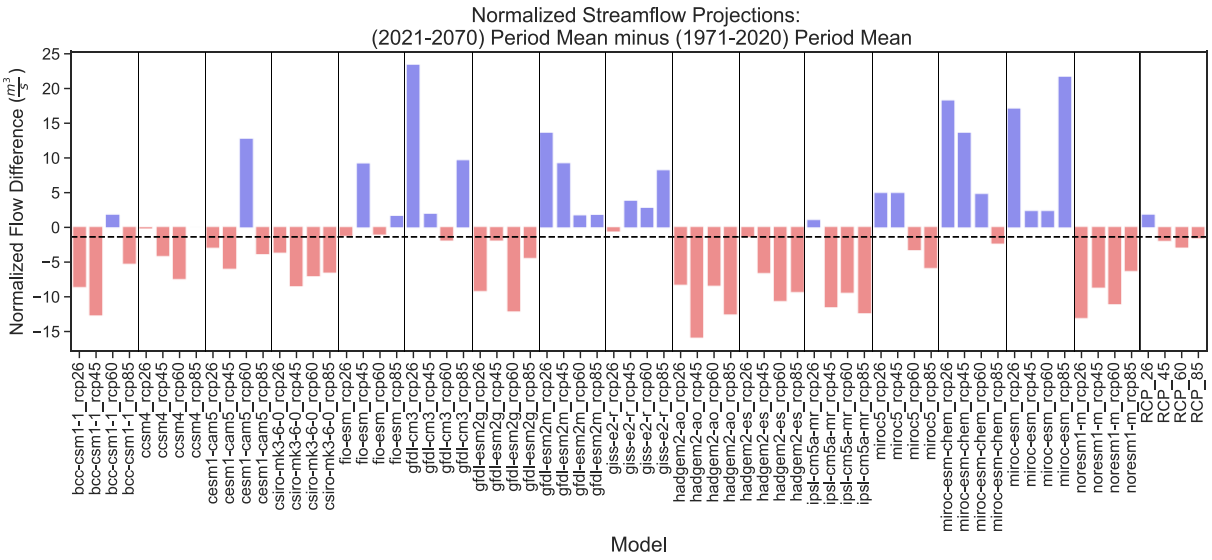

Figure 1.7. Differences in 50-year means (2021-2070) minus (1971-2020) of normalized flows for 16 different models, each forced by 4 different emissions scenarios (Table 1). Negative numbers reflect decreases in flow in the later period; blue bars indicate increases in flows. The mean across the 64 simulations, approximately -1 m^3/s, is shown as a horizontal black dashed line. The 16-member ensemble average difference for each of the four RCP scenarios is shown on the far-right side of the barplot.

Figure 1.8 16 model ensemble using normalized streamflow by RCP scenario.

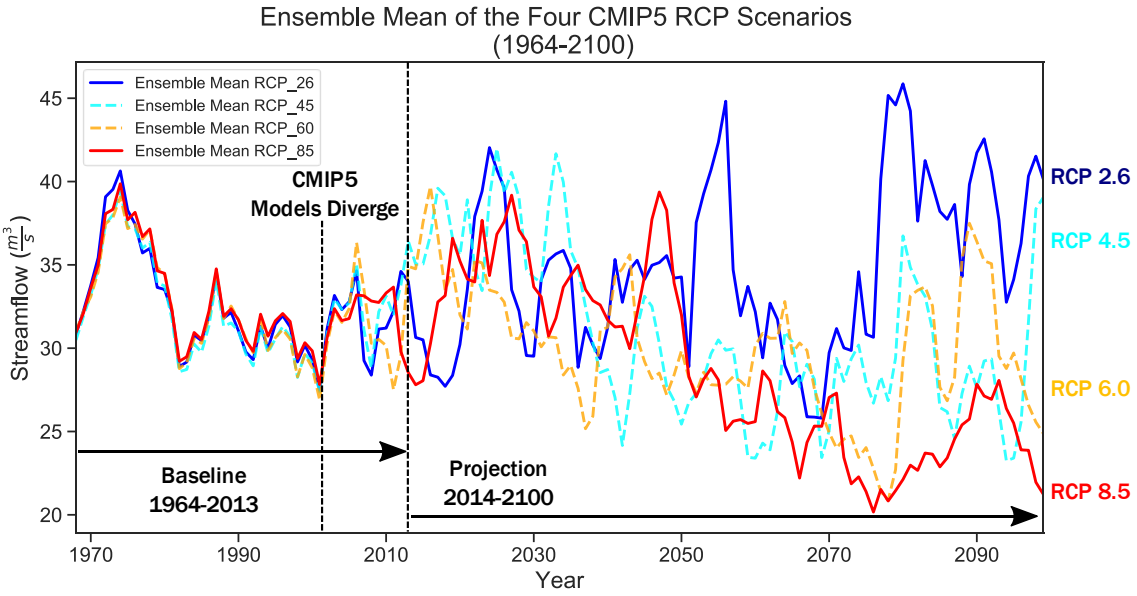

Figure 1.8. Ensemble mean of each RCP scenario averaged over the 16 models containing projections for all four RCP scenarios, as seen in Figure 7. The timeseries are smoothed using a 5-year running average.

Chapter 2: Assessing Water Management Strategies

I. Motivation and Objectives

In October 2018 Elephant Butte (EB) Reservoir was at 3% of capacity, or roughly 60,000 acre feet (https://waterdatafortexas.org/reservoirs/individual/elephant-butte). The lack of water in storage at EBR was cause for great concern among water users in New Mexico, Texas, and Chihuahua. EBR is the major storage reservoir for the Rio Grande Project, serving water users in the Rio Grande Valley downstream as far as El Paso and Juarez (Fig. 2.1). Just to the south of EB, at the outlet of Caballo reservoir, water is released to downstream users in Texas and Mexico to meet delivery requirements. Caballo releases are based on how much water in storage has been allocated to Texas and Mexico based on San Marcial inflows and the previous year's reservoir storage.

As a result, the way water is managed is a critically important issue for all who rely on the Rio Grande. Current drought conditions serve as a key motivation to analyze different water management strategies in response to observed and future inflows.

The San Marcial normalized inflow scenarios (Chapter 1) are used in this chapter as the primary input to a water balance model to evaluate strategies to manage the water south of the San Marcial gage, especially the water that is stored in EBR. The water balance model is run in predictive mode to discern the effects of different inflow scenarios on metrics such as reservoir storage, reservoir evaporation, and Caballo releases. We also explore changes to the model parameters, in order to compare output

metrics to those resulting from default settings, to evaluate the effect of various water management policy options.

In this chapter I evaluate how long it might take to fill EBR from historically low levels and explore water management strategies based on future inflows, as calculated in Chapter 1, or inflows based on observations, or synthetic inflow scenarios. The management strategies to be considered include maintaining a minimum amount of water in EB reservoir, reducing direct reservoir evaporation, and increasing San Marcial inflows.

I will evaluate the tradeoffs for each strategy and see which strategy may be most effective at increasing Caballo releases for downstream users, for example. It is evident there may be real-world barriers to some of these water management strategies given longstanding institutional, legal, and economic constraints. The validity of these options in this sense is beyond the scope of this paper. Instead, the management options evaluated in the water balance model are explored purely as a scientific exercise in potential management choices.

II. Methods

II.A. Study Area and Hydrologic Network

Figure 2.1 shows the project study area in southern New Mexico, far western Texas, and the northern section of the Mexican state of Chihuahua, including the six sub-watersheds comprising the study area and the Rio Grande channel. Runoff from the sub-watersheds is routed to nodes along the Rio Grande channel (Figure 2.1). The names,

areas, and runoff routing node for each sub-watershed are found in Table 2.2. The watershed boundaries were constructed by joining watersheds on the US side corresponding to HUC-8 watersheds in the USGS Watershed Boundary Dataset (USGS n.d.) and the "Cuenca" boundaries in Mexico (Conagua n.d.).

Water management options are assessed using a simplified water balance model developed at Michigan Technological University by Prof. Alex Mayer. The version of the water balance model used in this study includes four nodes, including the three watershed routing nodes: Caballo intermediate gage (CA), El Paso intermediate gage (EP), and Fort Quitman outlet gage (FQ). These three routing nodes, combined with the San Marcial inflow gage (SM), define three reaches of the Rio Grande channel, listed here from upstream to downstream: SM-CA, CA-EP, and EP-FQ. Each of these areas has its own simulated values of surface water, groundwater, and evapotranspiration. Only the first reach, SM-CA, which contains Elephant Butte and Caballo reservoirs, is considered for this study. In addition, Chapter 2 uses units of thousands of acre-feet (kAF) and thousands of acre-feet per year (kAF/year), which are standard operating units for water managers in this region. For context, one AF is equivalent to 43,560 cubic feet and one kAF/year is equivalent to an annual average flow of 1.38128 cubic feet per second (cfs).

II.B. Water Balance Model

II.B.1. Overall Mass Balance

A water balance model is based on conservation of mass, where water is the conserved quantity (Gleick 1987; Arnell 1999; Zhang et al. 2002; Singh 2016). The

model keeps track of inflows and outflows of water mass, to and from a set of control volumes, sometimes referred to as "buckets". In this case, the control volume can be reservoir or groundwater storage, such as Elephant Butte Reservoir. Mathematically, for a general case:

$$\frac{dS}{dt} = \sum I - \sum O \qquad (1)$$

where I is the sum of the inflows, O is the sum of the outflows, and $\frac{dS}{dt}$ is the rate of change in storage.

The surface water balance model simulates changes in storage, *dS/dt*, as

$$\frac{dS}{dt} = Q_{in} + Q_P - Q_{ET} - Q_{out} \qquad (2)$$

Q_{in} is the inflow at the upstream node of the reach; Q_P is the precipitation onto the sub-watersheds, Q_{ET} is the evapotranspiration from the sub-watersheds, and Q_{out} is the outflow at the downstream node of the reach. Storage volume, S, is usually constrained between prescribed minimum and maximum values: $S_{\min} \le S \le S_{\max}$. In the surface water balance model, equation 2 is solved in finite difference form over annual successive time steps, Δt, as in

$$\frac{S^t - S^{t-1}}{\Delta t} = Q_{in}^t + Q_P^t - Q_{ET}^t - Q_{out}^t \qquad (3)$$

where Δt = 1 year, S^t is the storage at the end of year t, and the flows, Q, are annual flows in year t.

Precipitation and evapotranspiration are divided into areal components for land surfaces (subscript *LAND*) and reservoir surfaces (subscript *RES*) as in

$$\begin{aligned} Q_P &= Q_{PLAND} + Q_{PRES} \\ Q_{ET} &= Q_{ETLAND} + Q_{ERES} \end{aligned} \quad (3)$$

Land surface areas are A_{LAND} and A_{RES}. Note that the Q_{ERES} subscript only refers to evaporation directly off the reservoir surfaces (see Section II.B.6). The runoff generated from the sub-watersheds, Q_{RO}, is calculated as

$$Q_{RO} = Q_{PLAND} - Q_{ETLAND} \quad (4)$$

which assumes that the residence time for groundwater in the sub-watersheds is shorter than 1 year. Groundwater is not considered in this version of the water balance model; in other words, there are no fluxes into or out of the surface water system from or to the groundwater system.

The preceding equations comprise the backbone of the surface water balance model. The surface water balance model is applied here in calibration and predictive and modes, as described in the following sections. The methods used to estimate the variables in these equations are described in the following sections.

II.B.2 Calibration Mode

Calibration of the water balance model is carried out by matching historical annual flows from the US Geological Survey at the three routing gages, Caballo Gage (USGS 08362500 RIO GRANDE BLW CABALLO DAM, NM), El Paso Gage (USGS 08364000 RIO GRANDE AT EL PASO, TX), and Fort Quitman Gage (USGS 08370500

RIO GRANDE AT FORT QUITMAN, TX,) for the calendar years 1994 through 2013. Historical annual inflow time series from the pair of SM gages is used to establish the upstream boundary condition (USGS 08358400 RIO GRANDE FLOODWAY AT SAN MARCIAL, NM and USGS 08358300 RIO GRANDE CONVEYANCE CHANNEL AT SAN MARCIAL, NM). The initial condition for reservoir storage, SRES0, established at December 31, 1993, is taken from US Bureau of Reclamation reservoir storage records (US Bureau of Reclamation n.d.). For the calibration of the SM-CA reach, the only fitted parameter is the reservoir pan evaporation coefficient, k_{pan} (shown in equation 6 below).

II.B.3. Reservoirs

There are two reservoirs in the SM-CA reach, Elephant Butte (EB) and Caballo. In both calibration and predictive modes, EB reservoir storage volume and surface area are determined every time step, but Caballo reservoir storage volume (5.74×10^4 AF) and surface area (3.38×10^3 acres) -- both much smaller than corresponding EB values -- are fixed at the historical mean, using daily data from the US Bureau of Reclamation (Bureau of Reclamation n.d.). The minimum and maximum EB volumes are 1.73×10^4 AF and 1.99×10^6 AF, respectively. Surface area to storage volume relationships ("hypsometric curves") for EB were fitted by digitizing hypsometric curves provided by the US Bureau of Reclamation (US Bureau of Reclamation 2008). Fourth-order polynomial series were sufficient to describe the surface area to storage volume relationship ($R^2 > 0.99$).

II.B.4. Precipitation

For the calibration over the historic period, annual precipitation rate time series for each sub-watershed were derived from a gridded dataset (Mauer et al. 2002; Livneh et al., 2015) of historical land surface fluxes for the study area. Precipitation rates are multiplied by respective land surface areas to calculate volumetric precipitation (Q_P). For predictive mode, precipitation rates are derived from the Bureau of Reclamation bias corrected and downscaled climate data from the climate dataset referred to in Chapter 1 (Reclamation 2013).

II.B.5. Runoff

For the historic period, annual runoff time series for each sub-watershed were derived from the same Livneh et al. (2015) data set of historical land surface fluxes for the study area. Livneh et al. (2015) used the Variable Infiltration Capacity (VIC) surface hydrologic model to estimate daily runoff and baseflow fluxes. These two fluxes were combined to determine Q_{RO}. For predictive mode, runoff constants, k_{RO}, were determined for each sub-watershed by regressing the annual time series for runoff against the annual time series for precipitation, for each sub-watershed, as in

$$Q_{RO} = k_{RO} Q_{PLAND} = Q_{PLAND} - Q_{ETLAND} \qquad (5)$$

This simple model eliminates the need to explicitly determine Q_{ETLAND}, such that the model is entirely driven by Q_{PLAND}. Note that this model ignores the portion of precipitation that infiltrates and eventually contributes to groundwater recharge, consistent with equation 4.

II.B.6. Evapotranspiration

The simple runoff model (equation 5) eliminates the need to explicitly estimate Q_{ETLAND}. The remaining component of overall evaporation is from the reservoir surfaces, estimated as

$$Q_{ERES} = A_{RES} e_{RES} = A_{RES} k_{PAN} e_{pan} \quad (6)$$

In calibration mode, e_{pan} comes from measurements at the EB climate station (www.ncdc.noaa.gov/cdo-web/search; https://www.ncdc.noaa.gov/IPS/cd/cd.html). In predictive mode, e_{pan} is simulated using the Hamon equation (Harwell 2012),

$$e_{RES} = 0.55 K_{Ham} \left(\frac{D}{12}\right)\left(\frac{SVD}{100}\right) \quad (7)$$

where K_{Ham} is a fitted constant, D is the number of daylight hours and SVD is saturated vapor density. The variable D depends on latitude; whereas SVD depends on local temperature. Derivations of D and SVD are found, for example, in Harwell (2012). The constant, K_{Ham}, was fitted from temperature and pan evaporation measurements at the EB climate station.

II.B.7. Predictive Mode

In predictive mode, inputs include annual time series for SM inflow, precipitation, and pan evaporation. The model then predicts flows at the CA node, which are also referred to here as Caballo releases. Caballo releases are determined based on a simplification of the 2008 Rio Grande Project Operating Agreement (Reclamation, 2008):

$$Q_{CAB} = \min(k_{CAB1}, k_{CAB2} Q_{SM}^{t} + k_{CAB3} S^{t-1}) \quad (8)$$

where the constants $k_{CAB1}, k_{CAB2},$ and k_{CAB3} are defined below:

$$Q_{CAB} \text{ constants:} \quad \begin{cases} k_{CAB1} = 875{,}000\ AF \\ k_{CAB2} = 0.56708 \frac{1}{AF} \\ k_{CAB3} = 0.46873 \frac{1}{AF} \end{cases}$$

The variable Q_{SM}^{t} is the annual inflow at the San Marcial node for the current year, and S^{t-1} is the reservoir storage at the end of the previous year. The first constant, k_{CAB1}, stipulates the maximum allocation from Caballo at 875,000 AF by way of the 2008 Operating Agreement. Flows that are less than k_{CAB1} are determined by the relative weights k_{CAB2} and k_{CAB3}. The first weight, k_{CAB2}, weighs the inflows to the San Marcial gage for the current year and the second weight, k_{CAB3}, weighs the end of year reservoir storage at the end of the previous year. Together the weights emphasize the relative importance of either the San Marcial inflow for the current year or the reservoir storage from the end of the previous year in determining the allowable release. The weights are derived based on a simplification of the 2008 Operating Agreement (Reclamation 2008).

In summary, the following section describes experiments with the water balance model that solves equation 3, for which S is EB+Caballo storage (with Caballo storage held fixed), Q'_{in} is annual San Marcial flow, and Q'_{out} is annual release downstream from Caballo Reservoir. The experiments describe several different inflow scenarios and several different adjustments to model parameters that represents water management options that affect calculations of Q_{ET} and Q'_{out}.

II.C. Modelling Experiments

II.C.1 Simulation of Historical Variability

The "default" water balance policy option we use as the control involves the parameters as outlined in Section II.B. The policy options here are run in the predictive mode where an inflow scenario is either based on historical inflows or future inflow scenarios. From Chapter 1, we focus on three future inflow scenarios: HAD85, ACC85, and MIR26, which depict a wide range of future projections. Precipitation and pan evaporation are prescribed in accordance with Section II.B.

The observed storage and observed Caballo releases can be compared to the modelled reservoir storage and Caballo releases when the model is driven with observed (1964-2013) inflows. The model is run in predictive mode and without altering any water balance model parameters, which is the default scenario (Figures 2.7-2.9). Figure 2.3 directly compares the modelled timeseries (dotted lines) to the corresponding observed timeseries (solid line). While the timeseries of observed and modelled are relatively similar, there are some key differences between the model output and the observations with regard to the difference in the magnitude of the reservoir storage and Caballo releases each year.

Figure 2.4 is a scatterplot of observed to modelled annual EB reservoir storage values. A red line indicates a perfect 1:1 linear fit. The model generally overestimates reservoir storage when storage values are low, and overestimates reservoir storage when storage is higher than 1000 kAF. At least some of the difference could be attributed to

water being managed differently in reality than the constrains represented by the model equations.

The same comparison is made between modelled and observed Caballo releases in Figure 2.4. Figure 2.4 reveals that the model overpredicts some of the lower release years and overpredicts the high flow years, such that the interannual variability of Caballo releases is underestimated. The maximum allowable release (see Section II.B.7.) shows up in the modelled output as dots along the 875 kAF/yr limit. The same maximum allowable release constraint is rarely met in the same year in the observed data. When the model projects the maximum allowable release, it consistently overpredicts Caballo releases relative to the observations. At least part of this systematic error could be attributed to using a simplified version of the 2008 operating agreement. Additionally, this timeseries mostly involves years prior to the existence of the 2008 Operating Agreement, meaning Caballo releases prior to 2008 may have been managed differently than dictated by the agreement.

The purpose of this section is to outline two different water management policy options and use the model to analyze the effectiveness of those options for mitigating hydrologic drought conditions. The first policy option maintains a 20% minimum storage threshold to keep more water in the reservoir. The 20% minimum storage value is approximately equivalent to 400 kAF. Operationally, when EB Reservoir contains more than 400 kAF of storage, water can be stored in upstream reservoirs (Article VII from the Rio Grande Compact; Reclamation 1939; Reynolds et al. 1974). This is a critical threshold because storing water upstream allows water to be stored in more favorable (cooler) reservoirs upstream, with lower reservoir evaporation rates. A

minimum storage threshold of 50% is also explored to see its effects on simulated EB storage, Caballo releases and EB evaporative losses. A full allocation in any of these policy options is 790 kAF as defined by the 2008 Operating Agreement (Reclamation 2008).

To set a minimum storage threshold within the bucket model a parameter called "reserve Elephant Butte storage" is set to 17.3 kAF (Section II.B.3). Under the default policy option, there are no changes to this parameter. Under the 20% minimum storage threshold, the reserve EB storage parameter is set to 400 kAF. The 50% minimum storage threshold has the reserve EB storage parameter set to 999.3 kAF.

The second management policy option involves reducing the reservoir evaporation parameter by 50%. Equation 6 shows that the reservoir evaporation in the model is a linear function of surface area. In order to reduce reservoir evaporation, the surface area is reduced by 50%. The interpretation is that the surface of the reservoir is covered with a material that reduces direct reservoir evaporation. The 50% reduction in surface area represents evaporation barrier that is covering 50% of the reservoir surface area. The method that could be used to do this is beyond the scope of this study, although we note that evaporative reduction surfaces have been implemented on smaller reservoirs.

II.C.2 Altering Inflow Scenarios

Inflow scenarios were developed in Chapter 1, based on a normalization procedure applied to future flows calculated from climate model projections by the BOR. We explored the hypothetical effects of increasing the quantity of water flowing into EB Reservoir by prescribing an increase in historical inflows by 10% or 25%. For the

observed run, this involved increasing the annual inflows over the baseline period by 10% and 25%. To obtain the effects of this increase on the normalized inflow scenarios, the increase was performed on the native observed flows and subsequently renormalized projected future flows in accordance with Chapter 1.

The basic premise of these increased flow simulations is the conceptual possibility that more water could be allocated to users downstream of EB Reservoir because of water management decisions within the state of New Mexico. Our consideration of this possibility does not constitute an endorsement of transferring water rights away from northern New Mexico rights holders; rather, we simply wish to use the model to advantage to explore a range of possible water management strategies, however unlikely they are to be implemented. We note that intrastate water management changes would not require a direct change to the Rio Grande Compact governing interstate water deliveries, or to the 2008 Operating Agreement that guides management within the Rio Grande project area downstream of EBR (Reclamation 1939; Reynolds et al. 1974, Reclamation 2008).

III. Results

Figure 2.1 is a map of the entire NIFA project study area. The scope of this paper is limited to only the Elephant Butte and Caballo watersheds (Reach 1; see Figure 2.2), and water balance model results are shown for only this reach. Figure 2.2 displays the watersheds (as a red outline) that are included in Reach 1 within the context of the water balance model. The San Marcial combined gages are located north of EB reservoir (as a green triangle) at the start of the EB watershed; this location is where the flow input to

the water balance model is defined. The Caballo gage is represented as a green triangle just south of the Caballo reservoir and at the southern extend of the Caballo watershed. As a result, the Caballo gage is where Caballo releases are defined within the water balance model.

Figure 2.6 is a water balance simulation showing the number of years it would take to completely fill EB Reservoir starting from 149 kAF (~6% of capacity) at the end of 2018 (not shown). The mean San Marcial flow for the historical period (1950-2013) was about 708 kAF/year; two times the average flow is about 1416 kAF/year which is above the 90^{th} percentile of annual flows for this period (Table 2.1). The dark blue line, from 2019-2022, illustrates the double the average San Marcial inflow condition and the pink line shows the increase in total reservoir storage (pink line) to the maximum storage value over this time period. Caballo releases (light purple line) are constant and meet the maximum release threshold from 2019-2025, after which they decrease. Direct reservoir evaporation is shown in green and increases with reservoir storage; reservoir evaporation peaks in 2022 at 350 kAF/year. It takes four consecutive years of two times the average inflow to completely fill EB reservoir from 6% of capacity. In the observed record (1950-2013), the highest combined San Marcial inflow observed over a four-year period averaged approximately 1482 kAF/year from 1984-1987. The same consecutive four-year period featured Elephant Reservoir reaching maximum capacity in the historical storage record.

Figures 2.6-2.12 are time series plots that share the same color scheme for each line and what the lines denote. However, Figures 2.7-2.12 show four sets of time series that use a common inflow scenario, with the four panels in each figure based on different

management scenarios: (a) the default policy option where no parameters have been altered; (b) the 20% minimum storage threshold; (c) 50% minimum storage threshold, and (d) reducing the direct reservoir evaporation by 50%. The line colors are associated with different water balance model inputs and outputs and are categorized as follows: San Marcial inflows (dark blue), total reservoir storage (pink), Caballo releases (light purple), change in storage from year to year (light blue), reservoir evaporation (green), input to Caballo (blue), and reservoir precipitation (light brown). The dashed horizontal red line indicates a full allocation (790 kAF), as described in the Methods section.

Figure 2.7 shows results of a dry inflow scenario based on observed San Marcial inflows from 2000-2013. Figures 2.7 through 2.8 use a starting storage volume of 154 kAF (not shown), which represents a low initial storage value, where the first inflow value is 400 kAF.

In the drought inflow default scenario (Figure 2.7) every year fails to meet a full allocation necessary to fully satisfy downstream users (top left panel). Visually, meeting a full allocation means that the Caballo releases (light purple line) are greater than or equal to the full allocation threshold (dashed red line). The 20% minimum storage policy option (top right panel) leads to higher storage values (pink line) and a decrease in Caballo releases (light purple line), relative to the default case, from 1999-2003 and 2012-2013. A full allocation was not met in this under this policy option. Additionally, there is a slight increase in reservoir evaporation (green line) over the time periods where the minimum threshold value is enforced (1999-2004 and 2012-2013) because more water is held in storage relative to the default case. Maintaining a minimum storage threshold of 50% (bottom left panel) causes a substantial increase in the reservoir storage,

as evidenced pink line and the increase relative to the default case. Again, with the increase in storage there is a corresponding increase in reservoir evaporation (green line) and a decrease in Caballo releases (light purple line). During the higher inflow years in 2005 and 2008 the emphasis on maintaining a 50% minimum storage threshold allow for a full allocation to be met during both years. However, Caballo releases (light purple) decreased across most of the timeseries, which is seen when the Caballo releases are compared to releases under the default case. The policy option that reduces reservoir evaporation (lower right panel) exhibits increases in reservoir storage (pink line) and enhanced Caballo releases (light purple) across the time series in relation every other policy option. A full allocation is achieved during 2005 and 2008 under this policy option.

The wet inflow scenario uses historical inflows from 1981-1989 (Figure 2.8). Under the default case (top left panel), San Marcial inflows (dark blue line) are increasing from 1981-1986. Maximum storage (pink line) is exceeded in achieved in 1986-1987, which is shown by the flattening of reservoir storage line for both years at the maximum value. The Caballo release (light purple) in 1987 is greater than the maximum allowable Caballo release value of 875 kAF. When flows exceed the reservoir storage threshold and excess water is in the system, the excess water overflows as additional Caballo releases. Again, the reservoir evaporation (green line) increases with the rise in reservoir storage. The 50% minimum reservoir storage threshold policy option (lower left) demonstrates that storage values will increase, and less water is available for Caballo releases for 1980-1982 relative to the default case. From 1983-1985 the storage values are higher overall and both 1986-1987 have excess Caballo releases due to spillage. The policy option

reducing reservoir evaporation (lower right panel) shows an increase in both reservoir storage and Caballo releases across the time series. When inflows decrease again from 1987-1989, the reservoir storage decreases less rapidly that it did for the other policy options. In fact, 1988 is an additional year where the reservoir was at maximum capacity. The water that spills during the Caballo releases (light purple line) in 1986-1987 is also greater in magnitude than the overflow during the 50% minimum storage threshold policy option.

Figure 2.9 uses the observed baseline period (1964-2013) as inflows to the water balance model. In general, the inflows (dark blue line) indicate a drier period from 1963-1978 and 1998-2013 with a wetter period from 1979-1997 in between. For the default case, a full allocation (found comparing pink line to red dashed line) was met 45% of time during the time series, most of which occurred during the wetter years from 1979-1997. When looking at the longer observed record the full magnitude of the interannual variability becomes apparent. The 50% storage threshold policy option (lower left) causes a decrease in Caballo releases (pink line) and an increase in reservoir evaporation (green) over the years when threshold is enforced; the threshold is enforced over the aforementioned dry years. When starting from 50% storage, the reservoir fills up more at the onset of the wetter years as seen in 1973 and 1978-1984, relative to the default case. However, overall Caballo releases are decreased and reservoir evaporation increases meaning a full allocation is only met 42% of the time, a decrease of 3% relative to the default case. A 50% reduction in reservoir evaporation (lower right panel) leads to additional Caballo releases and increased reservoir storage across both wetter and drier periods (as previously mentioned). Full allocation occurrences are met 50% of the time,

a 5% increase when compared to the default case. Minimizing evaporation losses off the reservoir especially helps during the wet periods, when more water is held in storage and there is more surface area. When transitioning from a wetter to a drier period from 1998-2003, for example, the reservoir maintains larger volumes of water during the period of drying and Caballo releases do not decrease as rapidly as they do under the other policy options.

The summary of these output metrics in Table 2.3 indicates that 29% of the volume of water entering the system at the San Marcial gages is lost to reservoir evaporation under the default observed inflow scenario. The ratio of Caballo releases to San Marcial inflows is about 88% under the same default inflow scenario. As higher storage minimum threshold values are imposed, the storage in Elephant Butte Reservoir increases, reservoir evaporation decreases, and Caballo releases decrease. As a result, the evaporation to inflow ratio increases to 36%, and the corresponding ratio of Caballo releases to San Marcial inflows decreases to 79%.

Table 2.4 shows the same pattern of effects of changing the model parameters as the observed inflow scenarios. The main difference between the observed and HAD85 inflow scenarios is that mean annual inflows under the HAD85 scenario are about 240 kAF/year less than the observed inflows used in Table 2.3. So, most of the difference between the observed and HAD85 inflow scenario is related to the lesser volume of water entering the system under the drier HAD85 inflow scenario than the observed inflow scenario. Therefore Table 2.4 illustrates negative percent change values when compared to the observed inflow scenarios. Again, about 1/3 of the inflows under the default

scenario are lost to evaporation, and this ratio of evaporative loss increases as the minimum storage threshold increases.

Figures 2.10 to 2.12 showcase the normalized flows, calculated in Chapter 1, as the inflow boundary condition for the water balance model. All climate influenced inflow scenarios here use the future inflow values from 2020-2070 as input to the water balance model. In each case, the initial reservoir storage is set to 415 kAF, or about 20% reservoir storage, in the water balance model. This value represents a low starting storage value for the water balance model runs to start from.

Figure 2.10 is a dry inflow scenario (ACC85) across most of the timeseries, except in 2061 when inflows were about 859 kAF. The mean inflow for under inflow this inflow condition is 360 kAF/yr. For comparison, this mean flow value falls below the 30th percentile value in the observed record (Table 1). As a result, there is consistently low reservoir storage (pink line), caballo releases (light purple line), and reservoir evaporation values (green line) across the entire time domain given the default case. Under the same inflow scenario, a 50% minimum storage threshold (lower left panel) leads to more evaporation losses (higher green) and a decrease in Caballo releases (light purple line) across the timeseries. Reducing minimum evaporation by 50% (lower right panel) does modestly increase the annual storage and the annual Caballo releases. However, the future inflow scenario is so dry that a full allocation is still unable to be met. Not one year met a full allocation when adjusting the bucket model parameters as described.

Figure 2.11 is a less extreme dry inflow scenario (HAD85) where there is a wetter period from 2020-2028 and 2039-2040. Most of the timeseries is consistent with a drier period. The default case (top left) shows that full allocation is achieved 18% of the time

and occur during the wetter years (Table 2.4). The HAD85 scenario where the minimum storage is restricted by 50% (lower left panel), is represented by the stationary reservoir storage values (flat pink line) during the drier years when the threshold is maintained. While the reservoir storage is greater during the drier periods, relative to the default case, Caballo releases decrease and reservoir evaporation increases. Caballo releases reach a full allocation 18% of the time, with no change relative to the default case. Reservoir evaporation is reduced by 50% (bottom right) and fosters an increase in reservoir storage (pink line) and Caballo releases (light purple line). With this policy option a full allocation is met 24% of the time, which is a 6% increase from the default policy option. The instances where additional full allocation year occur tend to happen when transitioning from higher inflows to lower inflows. For example, a full allocation is met in 2021-2027 under the default case and from 2021-2030 following the 50% reduction in reservoir storage policy option.

Figure 2.12 is a wet inflow scenario (MIR26) where the mean annual inflow is approximately 1304 kAF/year. When compared to statistics seen in the observed record, 1300 kAF/year is above the 90^{th} percentile (Table 1). The Caballo releases (light purple line) persist at, or above, the full allocation threshold 86% of the time in the default case (top left panel). The inflows are high enough that Caballo releases spill over the reservoir, releasing excess water from 2021-2024, 2034, 2040-2043, 2055, 2059, and 2069-2070. Maintaining a 50% minimum storage (lower left panel) value leads to a full allocation 84% of the time, a 2% decrease from the default case. An annual full allocation year is lost in 2047 because the extra water held in storage evaporates because preference is given to maintaining reservoir storage. However, when direct reservoir

evaporation is reduced by 50% (bottom right panel), evidenced by the lowering of the green line, there is a 4% increase in the number of years a full allocation is met. The gain in additional allocation years occurs during the drier period from 2045-2050. When compared to the other policy options, Caballo releases increase (light purple line) across the entire time domain because the water that is normally lost to evaporation (green line) is remains in storage (pink line) and goes into increasing Caballo releases.

Figure 2.13 and 2.14 share the same structure. Each panel represents one of four inflow scenarios, the y axis represents flow and storage, and the x-axis reflects four different management scenarios, with the same output metrics depicted for each one. Figure 2.13 shows observation-based inflows that are used as the boundary condition to the model and Figure 2.14 uses normalized inflows based on climate projections outlined in Chapter 1. The bars indicate the following metrics: the dark green bar shows mean annual inflows (kAF/year), the light green bars represent mean annual Caballo releases (kAF/year), the pink bars show mean annual reservoir evaporation (kAF/year), and the light blue bars with diagonal lines represent the mean annual storage in kAF.

To begin, Figure 2.13 reveals a similar pattern occurs in all water balance model results when looking at the annual mean of the timeseries. Imposing a minimum storage threshold, in all four panels, leads to greater storage (blue bar). However, the threshold results in increased reservoir evaporation (pink bar) losses and decreased Caballo releases (light green bar). Reducing reservoir evaporation translates to increases in mean annual reservoir storage and increases in mean annual Caballo releases. It should be noted that the short-term water balance runs (top right, bottom left, and bottom right panels) are based off a shorter time window of inflow values that do not convey the full range of

interannual variability seen in the historical run (top left). Figure 2.14 exhibits the same pattern in model output when tweaking the same model parameters. The main difference is Figure 2.14 has water balance model output based on future climate influenced inflow scenarios (top right, bottom left, bottom right panels) generated in Chapter 1. Once again, as the storage threshold increases, indicated by the taller dashed blue bar, the mean Caballo release decreases (shorter light green bar) and the reservoir evaporation increases (taller pink bar). If reservoir evaporation is decreased (shorter pink bar), instead of maintaining a storage threshold, there is an increase in the reservoir storage (blue bar) and an increase in Caballo releases (light green bar).

Figure 2.15 examines two adjustments made to the inflow scenarios. The first is a 10% increase in inflows and the second is a 25% increase in inflows over the historical baseline period, as discussed in Sec. II.C.2. This increase in inflows is reflected in the progressively taller dark green bars in all four panels.

Under the 10% increase in inflows scenario (middle set of bars in each panel), all inflow scenarios show a 6-10% increase in Caballo releases as evidenced by the taller light green bars. Taller light blue bars denote increased mean reservoir storage, which leads to a subsequent rise in reservoir evaporation (taller pink bars). The same management scenario leads to a 0-4% increase in the number of years full allocation is met (not shown). A policy option that results in a 25% increase in inflows, shown by the series of bars furthest to the right on the x axis of each panel, leads to higher storage values (taller blue bar), increased Caballo releases (taller light green bar), and increased reservoir evaporation losses (taller pink bar). Across all four inflow scenarios, increases in Caballo releases ranging from 15-27%. Therefore, the number of years a full

allocation is met occurs 0.2 to 12% more than under the default case (not shown in figure).

IV. Discussion

To summarize the results water balance model experiments we have focused on output metrics including San Marcial inflows, Caballo releases, direct reservoir evaporation and total reservoir storage. By assessing these four metrics, we can get a grasp of tradeoffs water managers could face in the future. We compare water balance model runs with different inflow conditions and by prescribing parameter adjustments within the water balance model to analyze water resources over time, especially pertaining to drought conditions.

Maintaining a minimum amount of water in storage demonstrates an attempt to prevent the reservoir from being almost completely drained, as occurred in 2018. The operational basis is Article VII of the Rio Grande Compact. This stipulates that EBR must contain at least 400 kAF (20% of the maximum storage) in order for water to be stored in upstream reservoirs, which is desirable because evaporation losses are less than they would be downstream at EBR. However, maintaining a minimum storage value every year comes at the expense of releases from Caballo for downstream users.

The reduction in water available for Caballo releases is due to the increased reservoir evaporation, caused by an increase in surface area. The increased evaporation is especially prevalent in the drier scenario and the minimum storage threshold strategy leads to more evaporation losses (Figures 2.7, 2.10, and 2.11). In the instances of the dry

scenarios, maintaining a 50% minimum storage threshold generally does not help meet allocation requirement as the water is lost to evaporation.

In other words, the attempt to reduce evaporation by storing water upstream through Article VII compliance is stymied by the increased evaporation associated with the greater surface area of EB Reservoir. In actual practice, when sufficient water is available in the Rio Grande system the BoR tries to maximize storage upstream in summer, when evaporation rates are highest, and then discharges flow downstream to EB Reservoir in late autumn. This sub-annual storage strategy cannot be simulated using the annual time step in the current version of the water balance model, but could be incorporated into future versions of the model using shorter time increments (e.g. monthly).

The minimum storage threshold under a wetter scenario has an effect similar to the dry scenario (Figures 2.8 and 2.12) in that the higher threshold causes more water to be held in the reservoir, hence more is subsequently evaporated. As a result, the Caballo releases decrease. While the strategy of maintaining a threshold, especially the 50% threshold, can help meet a full allocation for one or two additional years, the main effect is a loss in Caballo releases due to an increase in reservoir evaporation.

Reducing the direct reservoir evaporation by 50% was accomplished by prescribing a reduction in the surface area of the reservoir by 50%. The interpretation is that this is a layer of material is on the surface of the reservoir to prevent direct reservoir evaporation. Across all the inflow scenarios, reducing evaporation results in enhanced reservoir storage, increased Caballo releases, and an increase in the number of years a full allocation is met. In some instances, the number of years a full allocation was met increased by nearly 27 percent in the shorter timescale scenarios. The longer-term

scenarios saw a 0-6% increase in the number of years a full allocation was met. Under the dry scenarios, the method helped increase reservoir storage and increase Caballo releases.

However, the main issue was the lack of San Marcial inflows did not allow for sufficient volumes of water that fully satisfy downstream demand. The lack of inflows is especially apparent in the ACC85 climate inflow scenario (projecting a low flow future) where a full allocation is not met throughout the entire timeseries, despite attempts at making changes to the bucket model parameters.

While evaporation reduction is an appealing option from a modelling standpoint, we recognize that there are profound impediments to implementing these options. Assessing these impediments would require non-hydrologic analyses that are beyond the scope of this study. Some of the tradeoffs that would need to be studied in further detail are legal implications, economic considerations, tourism and recreational benefits that may be reduced, and environmental impacts.

Increasing the inflows by 10% and 25% helped increase reservoir storage and Caballo releases, but they also caused an increase in reservoir evaporation (Figure 2.15). However, mean annual Caballo releases did not increase uniformly across all scenarios. The wetter scenarios (Observed and MIR26) yielded enhanced Caballo releases due to spillage, resulting from storage that exceeded the maximum allowable storage that year. The number of years allocation was met increased under the wetter scenarios as well. Using observed inflows, the 10% increase in inflows policy option equated to a 4% increase in years a full allocation was satisfied and the 25% increase in inflows saw a 12% increase in years a full allocation was met (not shown in figure). The MIR26

scenario saw 2% and 4% increases in the number of years a full allocation was met for the same inflow increases. The ACC85 was unable to meet a full allocation during any year and the HAD85 10% and 25% increased inflow scenarios only increased the number of years there was a full allocation by 4% and 8%, respectively. Therefore, increasing inflows is a good way to meet full allocation under wetter scenarios or scenarios that have more interannual variability or lack of consecutive drought years.

This research only looks at the first reach of the study area (Fig. 2.1) and did not include results that analyzed the effects of groundwater changes in the water balance model. In downstream reaches the model includes equations that factor in the types of crops, evaporation off agricultural land, and groundwater pumping for consumptive use. Additionally, in the current version of the water balance model the precipitation and evaporation terms are calculated based on historical data from the Livneh dataset, not future local climate data. Future work should incorporate the local climate variables associated with the BOR BCSD 1/8-degree climate projections into the water balance model. These are all areas worthy of further investigation and study.

V. Conclusions

Future water management strategies are analyzed by using the normalized inflow scenarios from Chapter 1 as input to a simple water balance model. Reservoir storage, Caballo releases, and direct reservoir evaporation are the output variables of focus. Reservoir storage and Caballo releases reveal the amount of water that is available to downstream users, the water released to the downstream users, and how much of the demand was satisfied in any given year. Additionally, both output variables are one

indicator of hydrologic drought in the region. The reservoir evaporation tracks the losses of this water from the system as a function of reservoir surface area.

The projected inflows developed in Chapter 1 provide a wide range of future inflow scenarios that can be analyzed, indicative of the uncertainties of model projections of hydroclimatic change in this region. The large uncertainties inherent in these projections might seem to limit their usefulness. However, the main question is what can be done in drought years to maintain water resource in a way that allows for sufficient quantities of water for downstream users.

According to the water balance model results it takes about 4 consecutive years with double the average annual inflow (~1416 kAF/yr) to fill Elephant Butte Reservoir , assuming a starting reservoir storage value of 149 kAF (~6% of capacity), which is based on the reservoir storage value in December 2018. In other words, it takes four years of flows above the 90^{th} percentile of observed annual San Marcial flows from 1950-2013. This is not unprecedented in the historical record: the average observed combined San Marcial inflows from 1984-1987 evaluated to 1482 kAF/yr. This was the highest four-year consecutive average inflow recorded in the observed period from 1950-2013.

Establishing a minimum storage threshold decreases Caballo releases as the extra water stored is ultimately lost to evaporation and goes into maintaining the minimum storage threshold. In fact, even under the default inflow scenarios, about 1/3 of the water that entering the reservoir lost to evaporation (Table 2.3 & 2.4). Prescribing an increase of inflows (which would require unspecified decreases in water consumption upstream) helped to increase Caballo releases and reservoir storage, but also caused an increase in

direct reservoir evaporation. Reducing direct reservoir evaporation was helpful for increasing storage and increasing Caballo releases under wet and dry scenarios.

Even though some of these water management options could be helpful, it will be extremely difficult to manage water in a future where there are lower inflows from upstream areas as seen in most of the future scenarios in Chapter 1. The lower inflows are associated with higher emissions scenarios later this century, as seen in Figure 1.8. Furthermore, some drier scenarios also exhibit lower interannual variability in the future (e.g. ACC85 in Figure 2.10) so that there are fewer high flow years in future decades to replenish EB reservoir. The lack of sufficient water in the future is a real possibility with amplification of drought during the transition to a more arid climate in the southwestern United States. If there is less water to manage in the first place it will be difficult to satisfy delivery obligations even with the hypothetical management options considered in this chapter.

In this analysis, reducing evaporation seemed to offer the biggest promise for increasing reservoir storage and Caballo releases to meet full allocation. It should be noted that during a prolonged drought period, the water balance model suggests reducing direct reservoir evaporation helps retain more water in the reservoir for downstream users but is not substantial enough to satisfy the full allocation obligation. The magnitude of the volume of water flowing into EB reservoir is not sufficient to yield a full allocation to downstream users. Increasing the inflows at the San Marcial gage were effective in increasing Caballo releases but resulted in an increase of direct reservoir evaporation.

Tables

Table 2.1 San Marcial Streamflow Statistics (1950-2013)

Statistic	Flow (kAF/yr)
Maximum	1788.28
90th Percentile	1294.59
80th Percentile	1129.92
70th Percentile	970.70
60th Percentile	763.23
50th Percentile	575.87
40th Percentile	455.78
30th Percentile	406.43
20th Percentile	297.22
10th Percentile	243.09
Minimum	102.62
Median	575.87
Mean	707.98

Table 2.1. Percentile distribution of annual San Marcial flows (1950-2013).

Table 2.2 Subwatersheds and Routing System

Subwatershed	Area (acres)	River Reach Upstream Node	Runoff Routing and River Reach Downstream Node
Elephant Butte	1,400,468	San Marcial Gage	Caballo Gage
Caballo	793,751	San Marcial Gage	Caballo Gage
Jornada Draw	799,698	Caballo Gage	El Paso Gage
El Paso-Las Cruces	3,532,119	Caballo Gage	El Paso Gage
Rio Grande-Fort Quitman	1,813,138	El Paso Gage	Fort Quitman Gage

Table 2.2. Table showing the subwatersheds and their respective areas based on HUC-8 USGS watersheds. It also shows the respective upstream and downstream nodes that are defined within the respective subwatersheds.

Table 2.3 Observed Inflow Scenario Summary Statistics

Inflow Scenario: Observed	Mean Res. Evaporation (kAF/year)	Mean Res. Evap.: Mean Inflow (Ratio)	Mean Caballo Release (kAF/year)	Mean Cab. Release: Mean Inflow (Ratio)	Percent of Years Satisfying a Full Allocation (%)
Default	217.9	0.29	660.9	0.88	45.1
20% Min Res. Storage	222.1	0.29	654.9	0.87	45.1
50% Min Res. Storage	274.7	0.36	595.4	0.79	41.2
50% Reduction Res. Evap.	128.3	0.17	739.7	0.98	50.1

Table 2.3. Summary of results from the observed inflow scenario. Mean reservoir evaporation and mean Caballo releases are shown and the ratio of both variables to the mean annual inflow. The final column shows the percentage of years that meet a full allocation requirement.

Table 2.4 HAD85 Inflow Scenario Summary Statistics

Inflow Scenario: HAD85	Mean Res. Evaporation (kAF/year) (% Change)	Mean Res. Evap. / Mean Inflow (Ratio) (% Change)	Mean Caballo Release (kAF/year) (% Change)	Mean Cab. Release / Mean Inflow (Ratio) (% Change)	Percent of Years Satisfying a Full Allocation (%) (% Change)
Default	175 (-20%)	0.33 (14%)	483 (-27%)	0.90 (2.3%)	18 (-60%)
20% Min Res. Storage	191 (-14%)	0.36 (24%)	466 (-29%)	0.87 (0.0%)	18 (-60%)
50% Min Res. Storage	265 (-3.6%)	0.49 (36%)	387 (-35%)	0.72 (-8.9%)	18 (-56%)
50% Reduction Res. Evap.	103 (-20%)	0.19 (12%)	547 (-26%)	1.02 (4.1%)	24 (-52%)

Table 2.4. Same as Table 2.3, except this table shows values for the HAD85 inflow scenario. Percent changes are shown and represent the departure from the observed statistics seen in Table 2.3.

Figures

Figure 2.1 Overview of Study Area for the Water Balance Model.

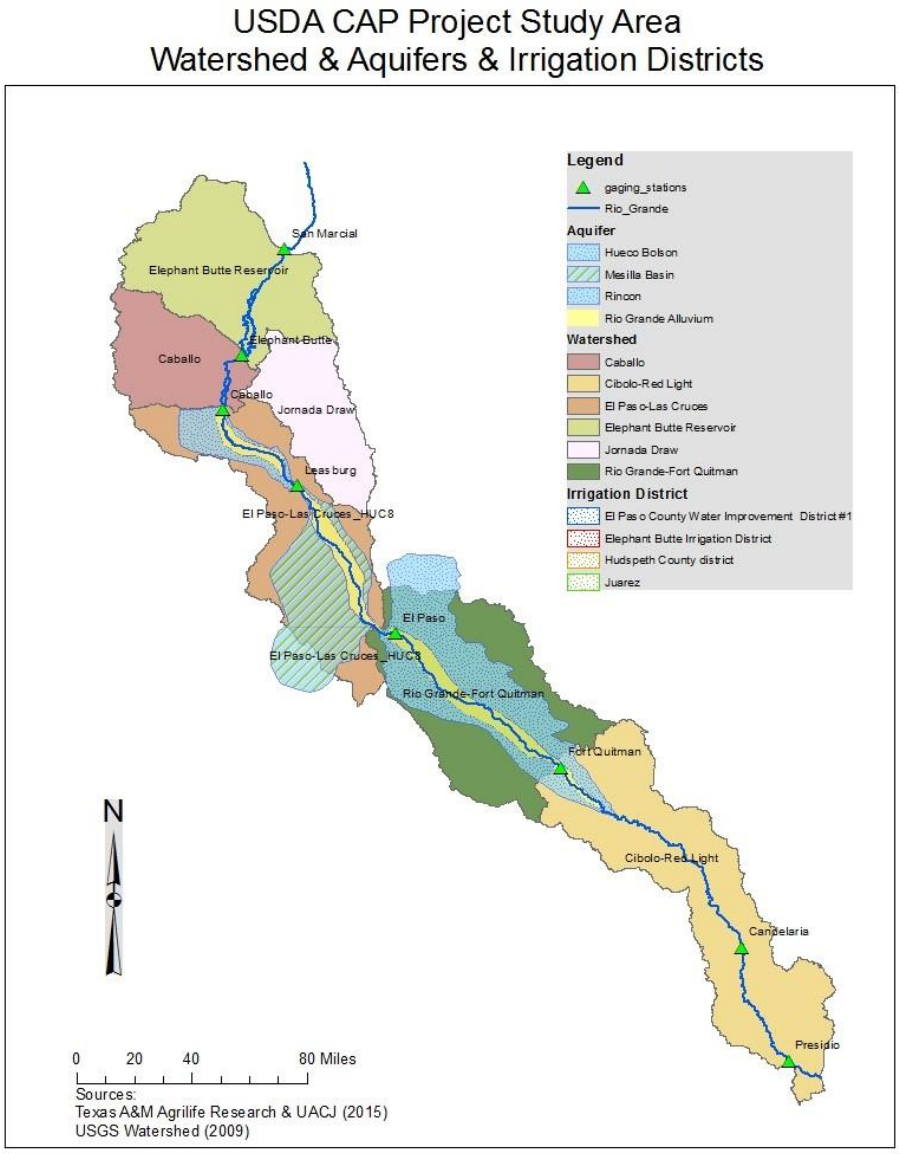

Figure 2.1. Overview of the entire NIFA study area. Gaging stations are the green triangles, watersheds are the solid colored polygons, and aquifers and irrigation districts are shown with hatching and stippled patterns. Top two watersheds (Elephant Butte and Caballo watersheds) are the focus of this chapter and comprise the region over which we calculate the water balance model output. Elephant Butte Reservoir is shown south of the San Marcial gage and the Caballo Reservoir is located just north of the Caballo gage and south of Elephant Butte Reservoir.

Figure 2.2 Overview of the Water Balance Model: Reach 1.

Figure 2.2. Overview of the water balance model area emphasized in this paper. The cities are shown as black dots with Albuquerque to the north and Ciudad Juarez to the south. The red outline delineates the EB and Caballo watershed (or Reach 1) in the water balance model. Reach 1 begins at the San Marcial gages (green triangle) at the upstream end of the EB watershed and ends at the Caballo gage (green triangle) at the downstream end of the Caballo watershed. The Rio Grande flows from north to south in this figure.

Figure 2.3 Model Performance Timeseries

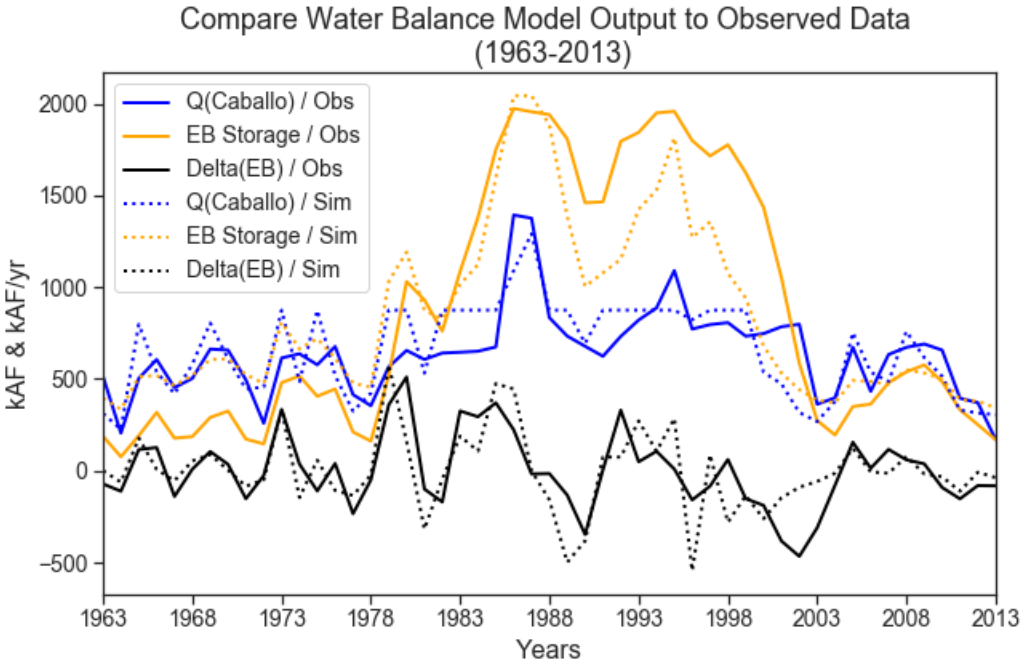

Figure 2.3. Timeseries comparing of the observed inflow scenario model output (dotted lines) to observations (solid lines). The variables compared are EB storage (orange), change in EB storage (black) and Caballo releases (blue). The figure is meant to an indication of model performance when compared to observed data over the baseline period.

Figure 2.4 Observed vs. Modelled EB Reservoir Storage

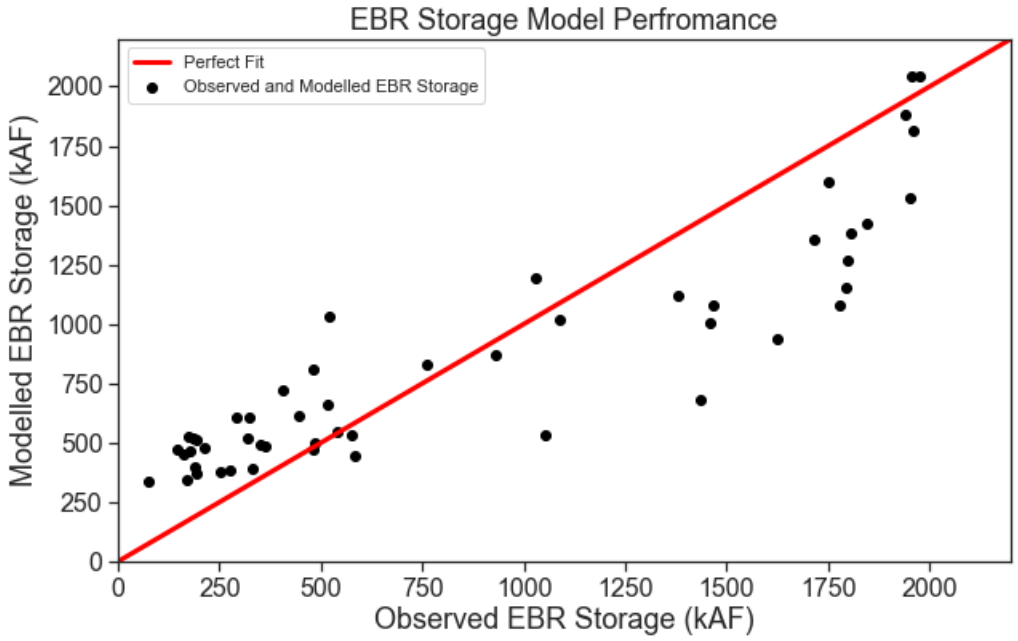

Figure 2.4. Timeseries plotting observed EB reservoir storage (x axis) versus modelled EB reservoir storage (y-axis) from the same observed inflow scenario shown in Figure 2.3. A perfect fit (1:1 ratio) is shown as the solid red line.

Figure 2.5 Observed vs. Modelled Caballo Releases

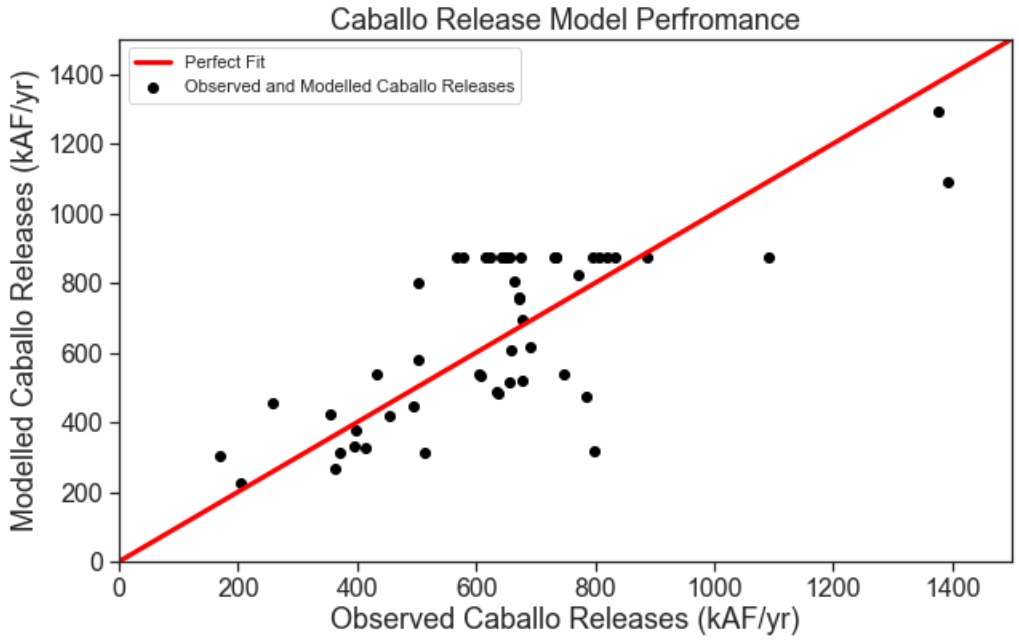

Figure 2.5. Timeseries plotting observed Caballo releases (x axis) versus modelled Caballo releases (y-axis) from the same observed inflow scenario shown in Figure 2.3. A perfect fit (1:1 ratio) is shown as the solid red line.

Figure 2.6 Future Flows that Would Fill Elephant Butte Reservoir from Dec. 2018 Initial Conditions

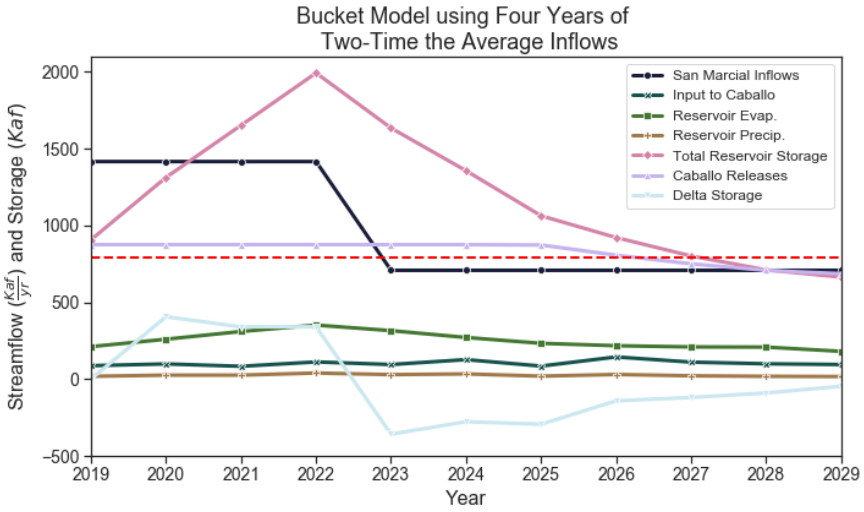

Figure 2.6. Annual time series of water balance model input (San Marcial inflows) and model output (Caballo input, reservoir evaporation, reservoir precipitation, total reservoir storage, Caballo releases, and change in storage). San Marcial inflows represent a prescribed scenario in which twice the average annual historical flow occurs the first four years (2019-2022) followed by six years of historically average annual inflows (2023-2029). The average flow is based on historical combined San Marcial inflow (from both streamgages) for 1950-2013.

Figure 2.7 Effects of Different Water Management Strategies During a Recent Period of Low Inflows

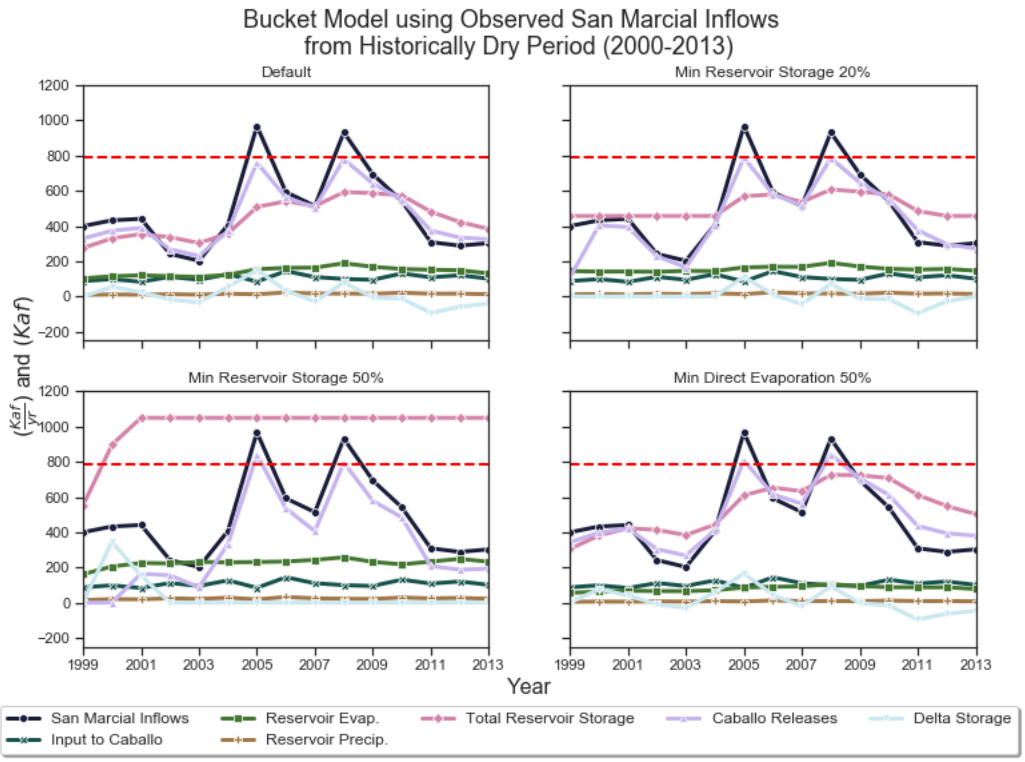

Figure 2.7. Annual time series of water balance model input (San Marcial inflows) and model output (input to Caballo, reservoir evaporation, reservoir precipitation, total reservoir storage, Caballo releases, and change in storage). The inflow condition is a dry period based on observed San Marcial inflows from 2000-2013. The top left panel represents no changes to the bucket model parameters and maintains the default settings. The top right panel set a 20% minimum storage threshold to try force the model to maintain that storage. The bottom left panel was the same except using a 50% minimum storage threshold. Lastly, the bottom right panel shows results when the direct evaporation off the reservoir is reduced by 50%.

Figure 2.8 Effects of Different Water Management Strategies During a Recent Period of High Inflows

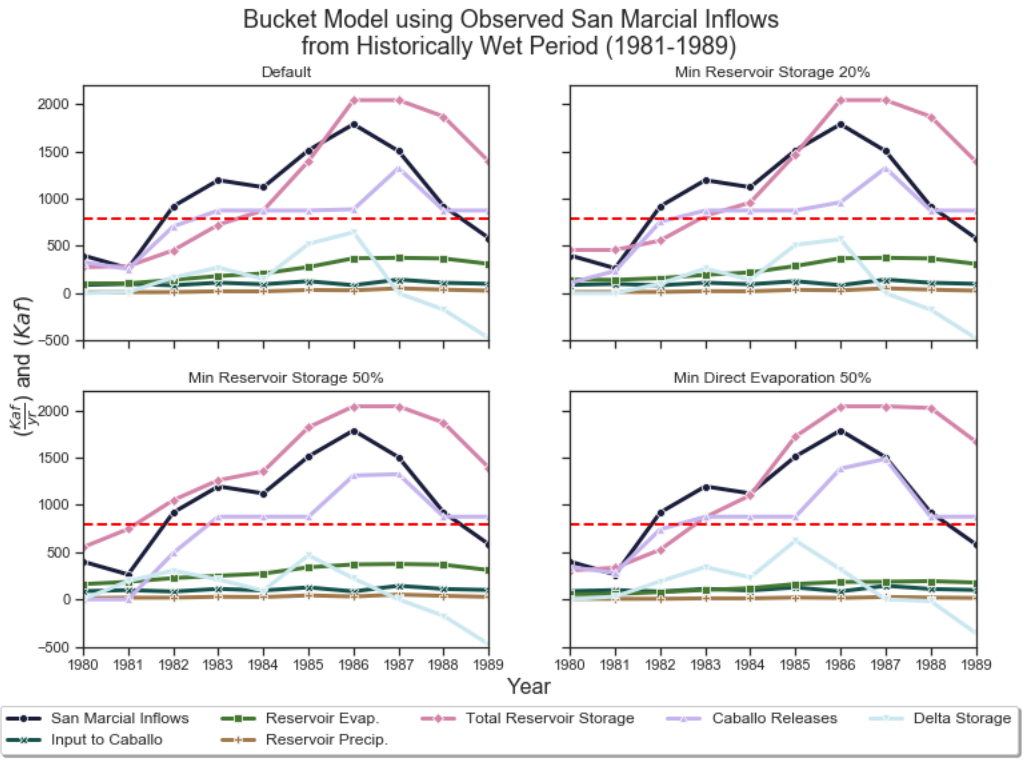

Figure 2.8. Like Fig. 2.7, but the inflow condition is a wet period based on observed San Marcial inflows from 1981-1989.

Figure 2.9 Effects of Different Water Management Strategies During the 50-year Baseline Period

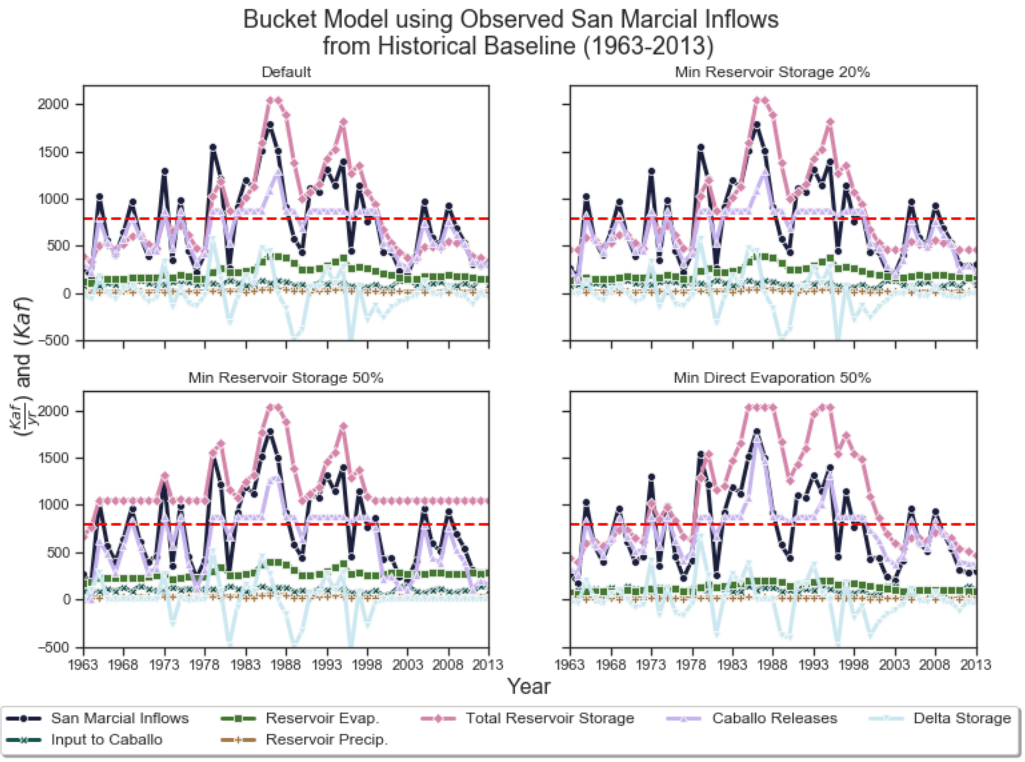

Figure 2.9. Like Fig. 2.7, except the inflow condition uses observed combined San Marcial gage flows from the historical baseline period (1964-2013).

Figure 2.10 Effects of Different Water Management Strategies on Projected Future Inflows: ACC85 Simulation

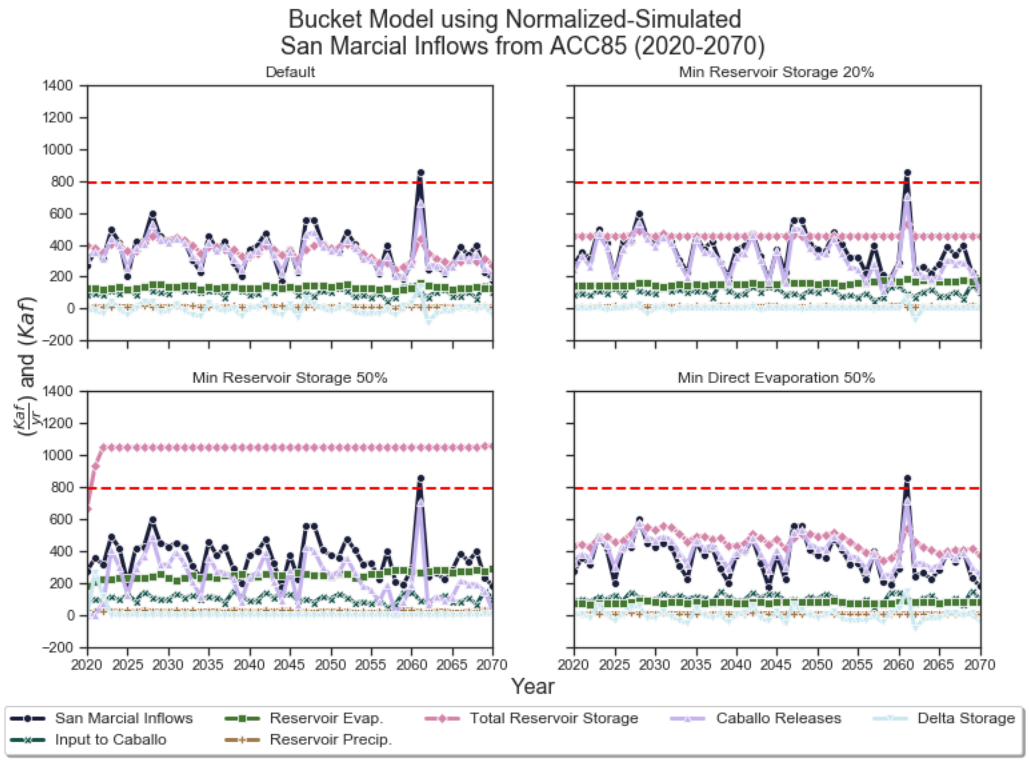

Figure 2.10. Like Fig. 2.7, except the inflow condition uses the ACC85 normalized streamflow values (calculated in Chapter 1) for 2020-2070.

Figure 2.11 Effects of Different Water Management Strategies on Projected Future Inflows: HAD85 Simulation

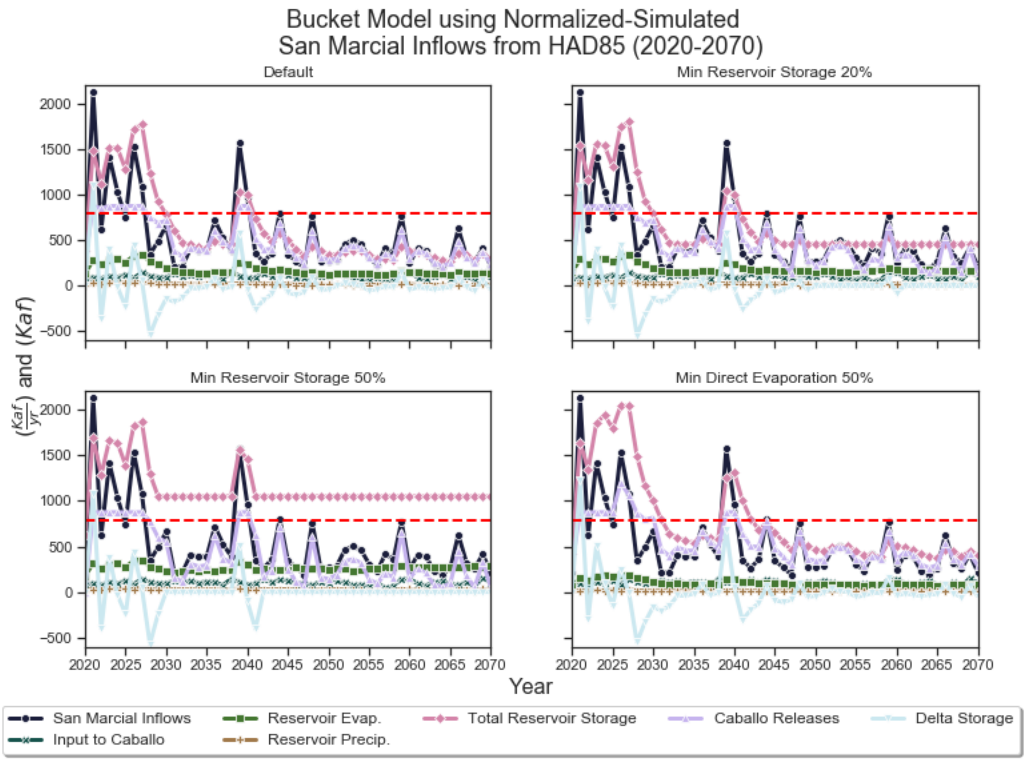

Figure 2.11. Like Fig. 2.7, except inflow condition uses the HAD85 normalized streamflow values (calculated in Chapter 1) for 2020-2070.

Figure 2.12 Effects of Different Water Management Strategies on Projected Future Inflows: MIR26 Simulation

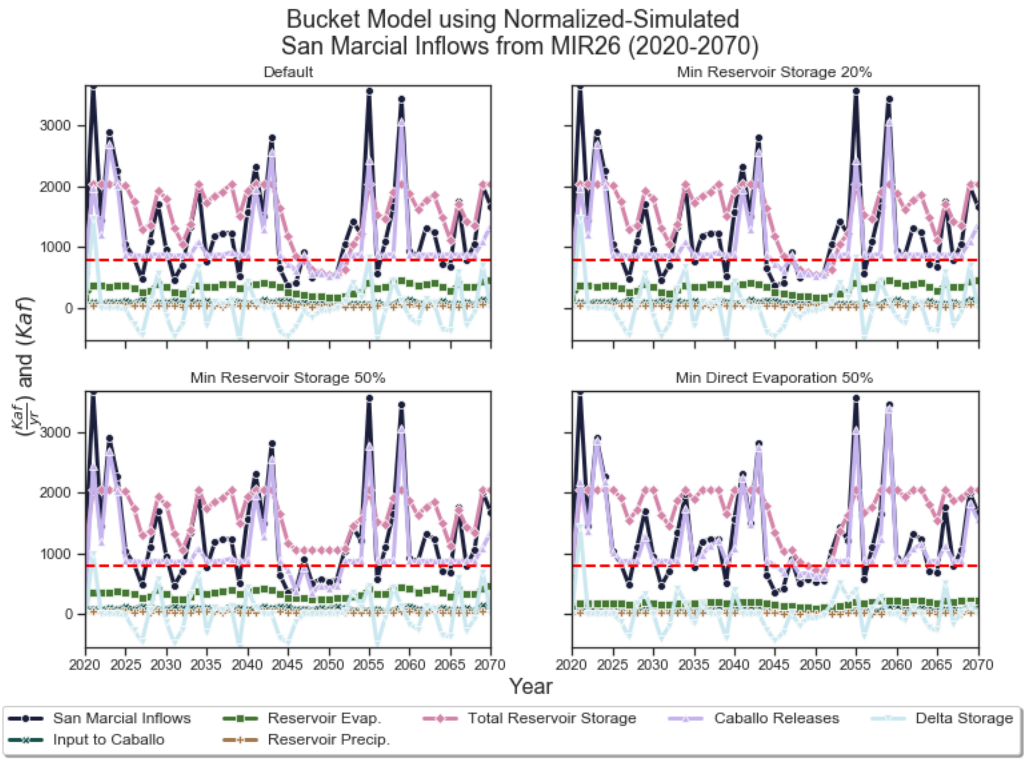

Figure 2.12. Like Fig. 2.7, except inflow condition uses the MIR26 normalized streamflow values (calculated in Chapter 1) for 2020-2070.

Figure 2.13 Summary Statistics for Observation Based Results

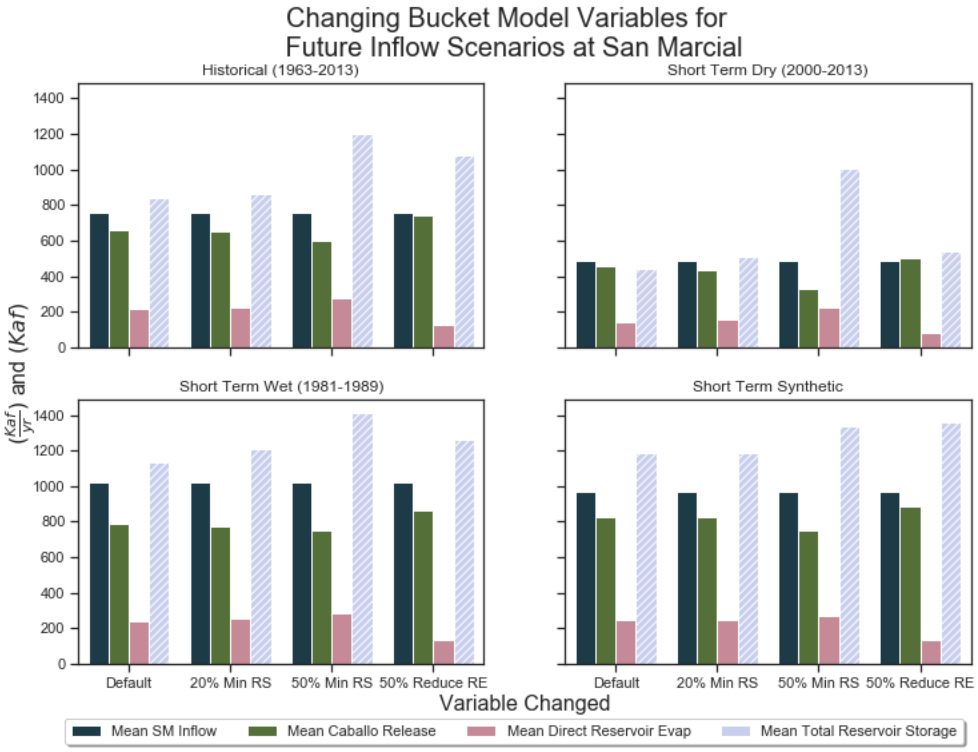

Figure 2.13. Bar charts illustrating the effects if changing parameters in the bucket model. Mean San Marcial inflow is the dark green bar, mean Caballo releases is the lighter green bar, mean reservoir evaporation is the pink bar, and the total reservoir storage is the hashed blue bar (in kAF). Each panel represents a different observation-based inflow scenario. The top left panel uses inflow values from the 1964-2013 historical period (Fig. 2.9). The top right panel based on the dry inflow values in Fig. 2.7. The bottom left panel used a historically wet inflow scenario from Fig. 2.8. The bottom right panel is based off the inflow scenario in Fig. 2.6. On the x-axis, each set of bars represents the variable in the bucket model that was changed. The left most set of bars is the default scenario, meaning no parameters were altered from the bucket model. The next set of bars to the right is where the minimum storage threshold of 20% was set. To the right of that is the 50% minimum reservoir storage value. Lastly, the furthest set of bars to the right represents a reduction of direct reservoir evaporation by 50%.

Figure 2.14 Summary Statistics for Observed and Normalized Inflow Scenarios

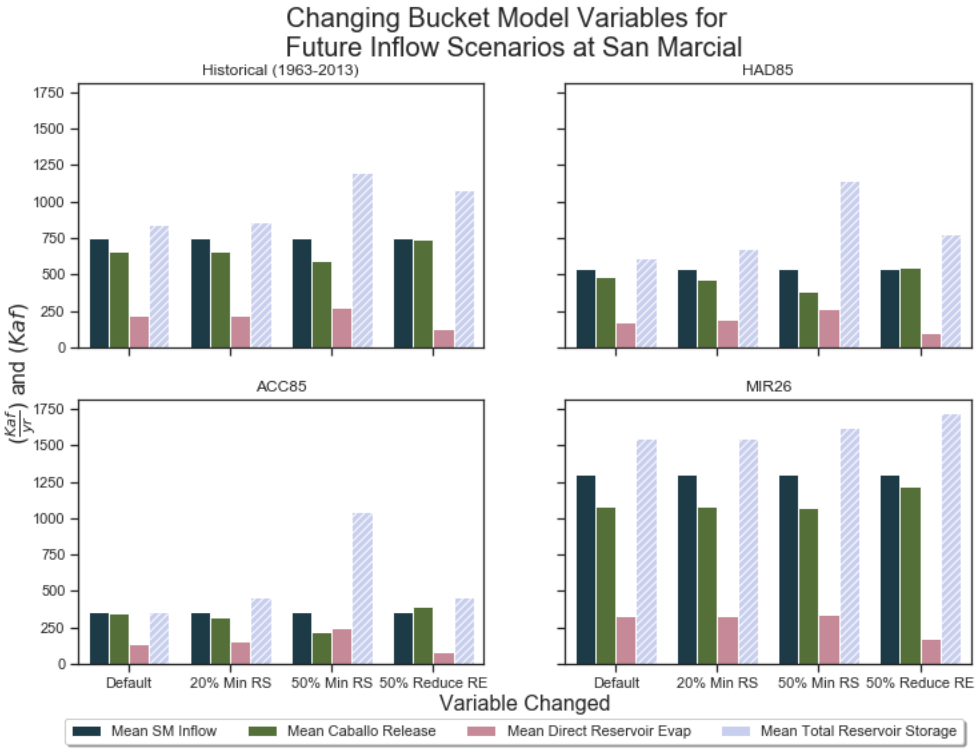

Figure 2.14. Same format as figure 2.13, except comparing normalized inflow scenarios (calculated in Chapter 1) for 2020-2070 for the HAD85 (top right; derived from Fig. 2.11), ACC85 (bottom left; derived from Fig. 2.10), and MIR26 (bottom right; derived from Fig. 2.12) scenarios to the observed inflow scenario (top left; derived from Fig. 2.9).

Figure 2.15 The Effects of Modifying Water Management to Increase Future Flows into San Marcial

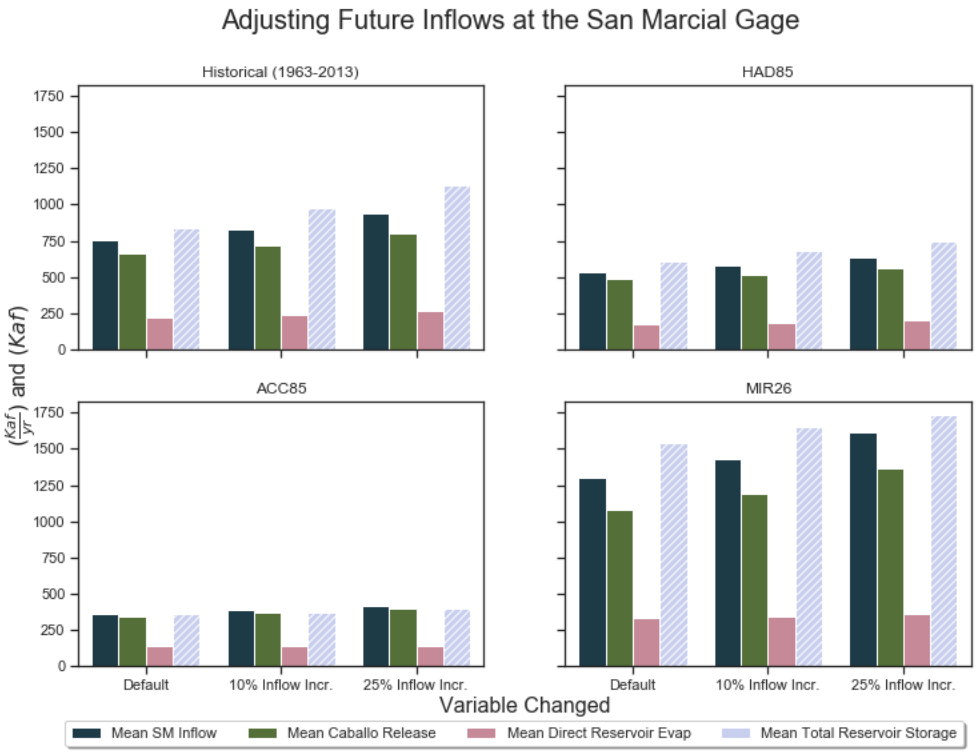

Figure 2.15. Same format as figure 2.13, except comparing normalized inflow scenarios (calculated in Chapter 1) for 2020-2070 for the HAD85 (top right), ACC85 (bottom left), and MIR26 (bottom right) scenarios to the observed inflow scenario (top left). This inflow parameter has been adjusted by 10% (middle set of bars) and 25% (right set of bars) and carried out through the normalized flows as well.

References Cited

Arnell N. W., van Vuuren D. P., M. Isaac. 2011. The implications of climate policy for the impacts of climate change on global water resources. Glob Environ Change 21(2): 592–603.

Blythe, T. L., and J. C. Schmidt. 2018. Estimating the natural flow regime of rivers with long-standing development: The Northern branch of the Rio Grande. Water Resources Research, 54(2), 1212-1236. https://doi.org/10.1002/2017WR021919.

Brutsaert, W. 2005. Hydrology: An Introduction. Cambridge University Press, 605 pp.

Conagua Comisión Nacional Del Agua. (n.d.). Sistema Nacional de Información del Agua. Retrieved from http://sina.conagua.gob.mx/sina/index.php?p=10, [Accessed 14 Jun. 2019].

Deser, C., R. Knutti, S. Solomon, and A. S. Phillips. 2012. Communication of the role of natural variability in future North American climate. Nature Climate Change, 2, 775–779.

Harwell, G.R., 2012, Estimation of evaporation from open water—A review of selected studies, summary of U.S. Army Corps of Engineers data collection and methods, and evaluation of two methods for estimation of evaporation from five reservoirs in Texas: U.S. Geological Survey Scientific Investigations Report 2012–5202, 96 p.

Howells, M., Hermann, S., Welsch, M. and Coathours. 2013. Integrated analysis of climate change, land-use, energy and water strategies. Nature Climate Change, 3(7), 621-626.

Hurd, B., and J. Coonrod. 2012. Hydro-economic consequences of climate change in the upper Rio Grande. Climate Research 53,103–118.

Gao, H.; Tang, Q.; Shi, X.; Zhu, C.; Bohn, T.J.; Su, F.; Sheffield, J.; Pan, M.; Lettenmaier, D.P.; Wood, E.F. 2010. Water budget record from Variable Infiltration Capacity (VIC) model. Algorithm Theoretical Basis Document for Terrestrial Water Cycle Data Records.

Gosling, S. M., Taylor, R. G., Arnell, N.W., and M.C. Todd. 2010. A comparative analysis of projected impacts of climate change on river runoff from global and catchment scale hydrological model. Hydrol. Earth Syst. Sci. Discuss. 7, 7191–7229.

IPCC, 2013: Climate Change 2013: The Physical Science Basis. Contribution of Working Group I to the Fifth Assessment Report of the Intergovernmental Panel on Climate Change [Stocker, T.F., D. Qin, G.-K. Plattner, M. Tignor, S.K. Allen, J. Boschung, A. Nauels, Y. Xia, V. Bex and P.M. Midgley (eds.)]. Cambridge University Press, Cambridge, United Kingdom and New York, NY, USA, 1535 pp, doi:10.1017/CBO9781107415324.

Jones, C. D. and Coauthors. 2011. The HadGEM2-ES implementation of CMIP5 centennial simulations. Geoscientific Model Development 4, 543-570.

Liang, X., D. P. Lettenmaier, E. F. Wood, and S. J. Burges. 1994. A Simple hydrologically Based Model of Land Surface Water and Energy Fluxes for GSMs, J. Geophys. Res., 99(D7), 14,415-14,428.

Livneh B., T.J. Bohn, D.S. Pierce, F. Munoz-Ariola, B. Nijssen, D. Cayan, R. Vose, and L.D. Brekki, 2015: Development of a spatially comprehensive, daily hydrometeorological data set for Mexico, the conterminous U.S., and southern Canada: 1950-2013, Nature Scientific Data, 2, 150042, doi:10.1038/sdata.2015.42

Mauer, E. P., Wood, A. W., Adam, J. C., Lettenmaier, D. P., and B. Nijssen. 2002. A long-term hydrologically-based data set of land surface fluxes and states for the conterminous United States. J. Climate, 15, 3237–3251.

Mix, K., V.L. Lopes, and W. Rast, 2012: Environmental drivers of streamflow change in the Upper Rio Grande. Water Resources Management 26:253–272.

Natural Resources Conservation Service (NRCS). 2011. National engineering handbook Part 622, Chapter 7: Water supply forecasting (19 p.) United States Department of Agriculture, Natural Resources Conservation Service. Retrieved from https://directives.sc.egov.usda.gov/OpenNonWebContent.aspx?content=32039.wba, accessed February 11, 2019.

National Centers for Environmental Information (NCEI). (n.d.). Climate Data Online, National Climatic Data Center (NCDC), www.ncdc.noaa.gov/cdo-web/search, [Accessed 6/18/2019].

National Centers for Environmental Information (NCEI). (n.d.). Climatological Data Publications, National Climatic Data Center (NCDC), https://www.ncdc.noaa.gov/IPS/cd/cd.html, [Accessed 6/18/2019].

Rio Grande Compact Commission Reports. New Mexico Office of the State Engineer / Interstate Stream Commission, Retrieved from www.ose.state.nm.us/Compacts/RioGrande/isc_rio_grande_tech_compact_reports.php, [Accessed 11/14/2018].

Pielke Sr., R. A. and R. L.Wilby. 2012. Regional climate downscaling: What's the point?, Eos Trans. AGU, 93(5), 52.

Reclamation. 2008. Operating Agreement for the Rio Grande Project, https://www.usbr.gov/uc/albuq/rm/RGP/pdfs/Operating-Agreement2008.pdf, [Accessed 4/1/2019]

Reclamation. 2013. Downscaled CMIP3 and CMIP5 Climate Projections Release of Downscaled CMIP5 Climate Projections, Comparison with Preceding Information, and Summary of User Needs. U.S. Department of the Interior, Bureau of Reclamation, 104 pp.

Reclamation. 2014. Downscaled CMIP3 and CMIP5 Climate and Hydrology Projections: Release of Hydrology Projections, Comparison with preceding Information, and Summary of User Needs, prepared by the U.S. Department of the Interior, Bureau of Reclamation, Technical Services Center, Denver, Colorado.

Reclamation. 2016. West-wide climate risk assessments: Hydroclimate Projections, Tech. Memo. 86-68210-2016-01, US Department of the Interior, Bureau of Reclamation, Technical Service Center, Denver, Colorado, 58.

Reynolds, S.E. & P.B. Mutz. 1974. Water Deliveries Under the Rio Grande Compact, 14 Nat. Resources J. 201.

Singh, V.P. 2016. Handbook of Applied Hydrology; McGraw Hill Professional: New York, NY, USA.

Taylor, K. E., Stouffer, R. J. and G. A. Meehl. 2012. An overview of CMIP5 and the experiment design. Bull. Am. Meteorol. Soc. 93, 485–498.

US Bureau of Reclamation. 2008. Elephant Butte Reservoir 2007 Sedimentation Survey Technical Report No. SRH-2008-4. Bureau of Reclamation, Denver, Colorado.

US Bureau of Reclamation (n.d.). Rio Grande Compact. [online]. Available from https://www.usbr.gov/uc/albuq/water/RioGrande/pdf/Rio_Grande_Compact.pdf. [Accessed June 7, 2019].

US Bureau of Reclamation. (n.d.). Upper Colorado Region. Retrieved from https://www.usbr.gov/rsvrWater/HistoricalApp.html [Accessed June 7, 2019].

United States Geological Survey. (n.d). Watershed Boundary Dataset. Available at: https://www.usgs.gov/core-science-systems/ngp/national-hydrography/watershed-boundary-dataset?qt-science_support_page_related_con=4#qt-science_support_page_related_con,[Accessed 14 Jun. 2019].

Woodhouse, C. A., G. T. Pederson, K. Morino, S. A. McAfee, and G. J. McCabe. 2016. Increasing influence of air temperature on Upper Colorado River streamflow, Geophys. Res. Lett., 43, 2174–2181.